TN
1877
c.1

NACA TN No. 1877

NATIONAL ADVISORY COMMITTEE FOR AERONAUTICS

TECHNICAL NOTE

No. 1877

c.1

EFFECTS OF COMPRESSIBILITY ON LIFT AND LOAD CHARACTERISTICS OF A TAPERED WING OF NACA 64-210 AIRFOIL SECTIONS UP TO A MACH NUMBER OF 0.60

By F. E. West, Jr., and T. Himka

Langley Aeronautical Laboratory
Langley Air Force Base, Va.

ENGINEERING DEPT. LIBRARY
CHANCE-VOUGHT AIRCRAFT
DALLAS, TEXAS

Washington
May 1949

MAY 27 1949

NATIONAL ADVISORY COMMITTEE FOR AERONAUTICS

TECHNICAL NOTE NO. 1877

EFFECTS OF COMPRESSIBILITY ON LIFT AND LOAD CHARACTERISTICS OF A TAPERED WING OF NACA 64-210 AIRFOIL SECTIONS UP TO A MACH NUMBER OF 0.60

By F. E. West, Jr., and T. Himka

SUMMARY

A wind-tunnel investigation of a tapered wing of NACA 64-210 airfoil sections and having an aspect ratio of 6 has been conducted at Mach numbers up to 0.60 in order to study the effects of compressibility on the lift and load characteristics. The range of angle of attack investigated was from about -4° up through the stall.

The maximum lift coefficient increased from a value of 1.02 at a Mach number of 0.15 to a low-speed peak value of 1.05 at a Mach number of 0.20; decreased to a value of 0.95 at a Mach number of 0.40; and then increased slowly to a value of 1.00 at a Mach number of 0.55, after which it increased rapidly to a value of 1.09 at a Mach number of 0.60 (limit of maximum-lift tests). At the higher Mach numbers and angles of attack, extensive regions of supersonic flow were formed over the forward part of the upper surface and resulted in large increases in lift coefficient; a peak local Mach number of about 1.78 was obtained at a free-stream Mach number of 0.60 and an angle of attack of 12.0°. As these large supersonic regions caused forward movements of the center of pressure, decreases in longitudinal stability occurred at the higher Mach numbers and angles of attack.

Mach number had only a slight effect on span-load distribution and on the shift of lateral center of normal force for angles of attack below the stall.

INTRODUCTION

For several years it has been known that both Reynolds number and Mach number affect maximum-lift characteristics of airfoils. This knowledge, however, has been based on only a few results obtained from wind-tunnel tests (references 1 and 2) and flight tests (references 3 and 4). With the speeds and altitudes flown by airplanes continually increasing, a

more extensive knowledge of these effects has become of importance both in the estimation of maneuvering and performance loads of high-speed airplanes and in the interpretation of wind-tunnel maximum-lift data as applied to the prediction of airplane characteristics at low speeds. Hence, an investigation of a series of fighter-type wings has been undertaken in the Langley 16-foot high-speed tunnel and in the Langley 19-foot pressure tunnel. The primary purpose of the investigation in the Langley 16-foot high-speed tunnel has been to study the effect of Mach number on maximum-lift characteristics up to a Mach number of 0.60; whereas, in the Langley 19-foot pressure tunnel, the primary purpose has been to study the interrelated effects of Mach number and Reynolds number on maximum-lift characteristics up to a Mach number of 0.35.

The first wing in the series to be investigated was composed of NACA 230-series airfoil sections and the second wing in the series to be investigated was composed of NACA 66-series airfoil sections. Both wings had 12-foot spans, taper ratios of 2:1, and aspect ratios of 6. The results of the investigation of these two wings are presented in references 5 to 10.

This paper presents the results of the maximum-lift investigation in the Langley 16-foot high-speed tunnel for the third wing of the series. This wing had the same plan form as the first two wings and was composed of NACA 64-210 airfoil sections throughout.

In addition to maximum-lift characteristics, general lift and pitching-moment characteristics, representative span-load distributions, and pressure data are presented.

SYMBOLS

Free-stream conditions:

V_o	corrected airspeed, feet per second
a_o	speed of sound in air, feet per second
M_o	Mach number $\left(V_o/a_o\right)$
M_{cr}	Mach number at which speed of sound is attained locally at some point on wing
ρ_o	mass density of air, slugs per cubic foot
q_o	dynamic pressure, pounds per square foot $\left(\frac{1}{2}\rho_o V_o^2\right)$

p_o	static pressure, pounds per square foot
μ_o	coefficient of viscosity of air, slugs per foot-second
R_o	Reynolds number $\left(\rho_o \bar{c} V_o / \mu_o\right)$

Wing geometry:

S	wing area, square feet
b	wing span, feet
A	aspect ratio $\left(b^2/S\right)$
$\bar{c}$	mean geometric chord, feet (S/b)
x	chordwise distance measured from airfoil leading edge, feet
y	spanwise distance measured from plane of symmetry of wing, feet
c	airfoil chord at any spanwise station, feet
c'	mean aerodynamic chord, feet $\left(\frac{2}{S}\int_0^{b/2} c^2 dy\right)$
α	angle of attack of wing at plane of symmetry, degrees

Force data:

L	wing lift, pounds
C_L	wing lift coefficient $\left(L/q_o S\right)$

Pressure data:

p	local static pressure, pounds per square foot
P	pressure coefficient $\left(\frac{p - p_o}{q_o}\right)$
P_{cr}	pressure coefficient corresponding to a local Mach number of 1.00

c_n section normal-force coefficient $\left(\int_0^1 \left(p_L - p_U\right) d\left(\frac{x}{c}\right)\right)$

$\frac{c_n c}{\bar{c}}$ section normal-load parameter

C_N wing normal-force coefficient $\left(\int_0^1 \frac{c_n c}{c} \, d\left(\frac{y}{b/2}\right)\right)$

$\frac{y_{cp}}{b/2}$ position of lateral center of normal force, fraction of semispan $\left(\frac{\int_0^1 \frac{c_n c}{\bar{c}} \frac{y}{b/2} \, d\left(\frac{y}{b/2}\right)}{\int_0^1 \frac{c_n c}{\bar{c}} \, d\left(\frac{y}{b/2}\right)}\right)$

x_1 distance from leading edge of any spanwise station to line perpendicular to plane of symmetry and passing through 25-percent position of mean aerodynamic chord, feet

$c_{m_{x_1}}$ section pitching-moment coefficient due to normal force about a line perpendicular to plane of symmetry and passing through 25-percent position of mean aerodynamic chord

$\frac{c_{m_{x_1}} c^2}{\bar{c}^2}$ section pitching-moment parameter

$C_{m_{c'/4}}$ pitching-moment coefficient about 25-percent position of mean aerodynamic chord $\left(\frac{\bar{c}}{c'} \int_0^1 \frac{c_{m_{x_1}}}{\bar{c}^2} \, d\left(\frac{y}{b/2}\right)\right)$

Subscripts:

L	lower surface
U	upper surface
i	incompressible
c	compressible
max	maximum

MODEL

A diagrammatic sketch of the wing is shown in figure 1. The principal dimensions of the wing given in this figure are also included with other pertinent information in the following table:

Wing span, feet	12
Wing area, square feet	24
Aspect ratio	6
Taper ratio	2:1
Mean aerodynamic chord, feet	2.07
Airfoil section (see reference 11)	NACA 64-210
Sweepback (along leading edge), degrees	6.34
Dihedral (along quarter-chord line), degrees	0
Geometric twist (washout), degrees	1.5

In the left semispan of the wing, 35 pressure orifices were distributed over each of the six spanwise stations shown in figure 1. The wing was made of solid steel.

INSTALLATION

Force tests.- The basic force tests were run with the wing mounted upright on shielded support struts. (See fig. 2.) Tests were made with the wing inverted both with image struts (see fig. 3) and without image struts in order to obtain data for the determination of tare corrections.

Pressure tests.- Except for the addition of a boom and counterbalanced tail strut, the pressure-test installation shown in figure 4 was similar to that used for the basic force tests. Pressure tubes leading from the wing pressure orifices were conducted from the wing through the boom and counterbalanced tail strut to multitube manometers.

TESTS

For a Mach number range of 0.15 to 0.60, force and pressure data were obtained for a range of angle of attack of about -4° up through the stall. Tunnel drive power limitations prevented obtaining data at Mach numbers higher than 0.60 above an angle of attack of 6°.

Data for angles of attack up to 6° were obtained by maintaining a constant angle of attack and varying the tunnel speed. For higher angles of attack, the tests were run by keeping tunnel speed constant and varying the angle of attack in order to define the stall sharply.

The variation of the average test Reynolds number with Mach number is shown in figure 5.

CORRECTIONS

Force data.- The force data have been corrected for strut tares, air-stream misalinement, and tunnel-wall effects. The methods used in the determination of all force-data corrections are discussed fully in reference 5.

The strut tares were a maximum at the lowest angles of attack and became negligible at an angle of attack of approximately 7°. The largest increment of lift coefficient obtained from the strut tares was approximately 0.05.

The air-stream misalinement angle of 0.16° upflow used in the present investigation was determined by averaging the results obtained from the wing tests reported in references 5 and 8.

Lift forces were also corrected for pressure differentials measured across rubber diaphragms which were fitted around the strut shield bases to prevent air leakage through the shields. The force-test results were based on a tunnel-empty calibration.

Pressure data.- No corrections other than those applied to free-stream Mach number and angle of attack have been made to the pressure data presented in this paper. All pressure-test results were based on a tunnel-empty calibration.

Both free-stream Mach number and angle of attack were corrected by methods similar to those used for the force data. Normal-force coefficients (which were corrected for strut tares and blockage effects), however, were substituted for lift coefficients in the angle-of-attack corrections.

RESULTS AND DISCUSSION

Lift Characteristics

The general lift characteristics of the wing are shown in figure 6. In order to show the stalling characteristics more clearly at several Mach numbers, some of the curves of figure 6 are presented in figure 7.

Most of the lift curves are linear below stalling angles with the lift-curve slopes varying from 0.077 per degree at a Mach number of 0.20 to 0.091 per degree at a Mach number of 0.60.

Variation of lift coefficient with Mach number.- In order to give a clearer concept of the variation of lift coefficient with Mach number, data from figure 6 are presented in figure 8 along with calculated curves based on low-speed data extrapolated by a modification of the Glauert-Prandtl theory. (See reference 12.) This theory assumes that the induced velocities over the wing are small and, therefore, is strictly applicable only to a thin wing operating at low angles of attack. If a two-dimensional lift-curve slope of 2π is assumed, the theoretical increase of lift coefficient with Mach number is

$$\frac{C_{L_c}}{C_{L_i}} = \frac{A + 2}{2 + A\sqrt{1 - M_o^2}}$$

Figure 8 shows that for Mach numbers below the critical, good agreement exists between the experimental and calculated lift for angles of attack up to 10°. For Mach numbers above the critical, the agreement appears to be good up to an angle of attack of 8°. The values of critical Mach number in figure 8, which were determined from pressure distributions, may be high due to a lack of pressure orifices in the immediate vicinity of the leading edge. Figure 9 shows the effect of Mach number on pressure distributions at a representative spanwise station for an angle of attack of approximately 6.7°. As might be expected from the force data, no radical or large changes due to the effect of Mach number appear for the Mach number range investigated.

At supercritical speeds, however, figure 8 shows that for angles of attack above 8°, changes occur in the experimental lift coefficients that cause them to differ appreciably from the calculated lift coefficients. Upon first exceeding the critical Mach number the experimental lift coefficients for these high angles of attack are affected by changes in lift-curve slope (see fig. 6) and either remain approximately constant or decrease. In figure 10, which shows the effect of Mach number on the

pressure distribution at a representative spanwise station for an angle of attack of 11.0°, either more separation or a thicker boundary layer occurs over the trailing edge (evident from the decrease in pressure recovery at the trailing edge) for Mach numbers of 0.40 and 0.50 than for a low Mach number. These increases in separation or boundary-layer thickness at the trailing edge apparently have detrimental effects on the pressures over the upper surface. (See, for example, fig. 12(b).) Figure 10 also shows that the contributions of the lower surfaces to the lift coefficient are less at Mach numbers of 0.40 and 0.50 than at a low Mach number. Thus, the changes that occur in the lift coefficients when the critical Mach number is first exceeded appear to be due to separation or thickening of the boundary layer at the trailing edge and to lower pressures over the lower surface.

For Mach numbers higher than 0.50, figure 8 shows that the lift increases rapidly at the high angles of attack. Figure 10 shows that at these high Mach numbers large regions of supersonic flow are formed over the forward part of the upper surface. At a Mach number of 0.55 a large region of supersonic flow becomes evident along with a well-defined shock that is indicated by the rapid change from the supersonic flow condition to the subsonic flow condition. As the Mach number is increased to 0.60, the shock moves rearward and the extent of the region of supersonic flow along the chord increases from 12 percent to 25 percent of the chord. Thus, the large increases with Mach number in lift coefficient at high Mach numbers and angles of attack are associated with the formation of large regions of supersonic flow over the forward part of the upper surface that cause large area increases in the pressure distributions. The large size of these regions of supersonic flow may partly be attributed to the comparatively sharp leading edge of the wing. That is, at higher angles of attack much higher accelerations of flow occur about the noses of comparatively sharp leading-edge airfoils, such as the NACA 64-series, than occur about the noses of blunt leading-edge airfoils, such as the NACA 230-series. (See reference 8.)

Figure 10 also shows that with the occurrences of the well-defined shocks there are decreases in trailing-edge separation or a thinning of the boundary layer at the trailing edge.

Maximum lift coefficient.- The effect of Mach number on the maximum lift coefficient is shown in figure 11. Also shown in this figure are maximum normal-force coefficients for several Mach numbers. The maximum lift coefficient increases with Mach number from a value of 1.02 at a Mach number of 0.15 to a low-speed peak value of 1.05 at a Mach number of 0.20. Although Mach number has a slight effect in this speed range (see reference 7), this increase in maximum lift coefficient is essentially a Reynolds number effect. (For variation of average test Reynolds number with Mach number, see fig. 5.) Increasing the Reynolds number moves the

transition point forward along the chord and gives the flow more resistance to separation. Hence, an increase in Reynolds number allows higher values of lift and angle of attack to be reached before the occurrence of stalling. (See reference 13.)

After the low-speed peak value is reached, the maximum lift coefficient slowly decreases with increasing Mach number to a minimum value of 0.95 at a Mach number of 0.40. The reason for this decrease may depend on whether or not the peak pressures at the leading edge reached or exceeded the critical pressure coefficient. The pressure distributions for this wing show that the peak pressures did not reach the critical pressure coefficient at these low Mach numbers; but, as previously indicated, higher pressures might have been obtained if more pressure orifices had been located in the immediate vicinity of the leading edge. If the peak pressures did reach or exceed the critical pressure coefficient there is a possibility that slight shock disturbances may have precipitated leading-edge separation. (See reference 7.) For this condition, therefore, the maximum lift coefficient would decrease after the low-speed peak value has been reached inasmuch as the critical pressure coefficient would occur at lower angles of attack because of compressibility effects. If the peak pressures did not reach the critical pressure coefficient then the decrease was probably due to the favorable effect of Reynolds number being counteracted by compressibility effects in the form of large adverse pressure gradients in back of the peak pressure points that tended to induce separation from the leading edge. (See reference 14.)

With further increases in Mach number the maximum lift coefficient increases slowly up to a value of 1.00 at a Mach number of 0.55, after which it increases rapidly to a value of 1.09 at a Mach number of 0.60 (limit of maximum-lift tests).

Figure 7 indicates that pronounced separation of the flow exists over the wing at the maximum lift coefficients for Mach numbers of 0.45 and 0.50. A study of unpublished pressure distributions for these conditions showed that although pressures over the forward part of the upper surface were decreased because of the effects of trailing-edge separation, the pressures over the rear part of the upper surface increased sufficiently to cause an increase in lift over the upper surface. Hence, inasmuch as the contribution of the lower surface to the lift changed only slightly, the lift coefficients did not reach their maximum values until approximately 10° above the angles of attack where stalling first became apparent. Inasmuch as large increases in stability occur at these high angles of attack (see, for example, fig. 19), an airplane with a similar wing may not be able to reach the maximum lift coefficient at these Mach numbers because of limited elevator control. Also severe buffeting, which is likely to be present for these conditions, may limit the maximum lift coefficient obtainable in flight.

Figure 11 shows a dashed lift curve extending over a Mach number range of 0.40 to 0.55 that represents lift coefficients obtained approximately 2.5° to 3.5° above angles of attack where stalling first becomes apparent. This lift curve is believed to represent a more practical limit of the maximum lift coefficients obtainable in flight.

The increases in maximum lift coefficient for Mach numbers of 0.55 to 0.60 are associated with the occurrence of shock and the formation of extensive regions of supersonic flow over the forward part of the upper surface, previously discussed. Figure 7 shows that these high maximum lift coefficients are also associated with the wing stalling at higher angles of attack for Mach numbers of 0.55 and 0.60 than for slightly lower Mach numbers. These increases in the stalling angle probably occur because the shock has a delaying effect on the forward movement of trailing-edge separation.

Figure 11 shows that good agreement exists between the maximum lift and maximum normal-force coefficients at all values of Mach number except 0.60. An analysis of the data showed that at a Mach number of 0.60 the variation of lift and normal-force coefficients (unpublished data) with angle of attack were practically identical except that for the pressure tests the wing stalled at an angle of attack of about 0.7° higher than for the force tests. Approximately 10 percent of the difference between the maximum lift and normal-force coefficients at a Mach number of 0.60 occurs because no blockage corrections were applied to the normal-force data. However, the only apparent discrepancies existing between the force and pressure tests that could account for the difference in stalling angle are the addition of a boom and tail strut for the pressure test configuration and differences in free-stream relative humidity. Although calculations indicated that the free-stream relative humidities for the force tests were only 6 to 26 percent higher than the 89 percent determined for the pressure test, condensation (if it occurred) may have had a more detrimental effect on the flow over the wing for the force tests.

Stalling characteristics.- An examination of figures 6 and 7 appears to indicate that a knowledge of the stalling characteristics of the wing can be obtained by considering the low-speed stall ($M_o = 0.20$), the moderate-speed stall ($M_o = 0.40$), and the high-speed stall ($M_o = 0.60$). In order to show these stalling conditions, pressure distributions at a representative spanwise station are shown in figure 12 and pressure contours showing the stall progression over the upper surface of the wing are presented in figures 13 to 15.

Although the normal-force curve for a Mach number of 0.20 (which is not presented) shows a very slight rounding at the peak, the stall shown in figures 12(a) and 13 is believed to be also representative of

the stall indicated by the lift curve for a Mach number of 0.20 in figure 6. This low-speed stall, which occurs rather abruptly, appears to be associated with a combination of leading-edge and trailing-edge separations. Figure 12(a) shows that as the angle of attack is increased there is a rapid steepening of the pressure gradient in back of the peak pressures. This pressure gradient probably becomes so adverse that it precipitates the laminar separation that occurs near the peak pressure point for an angle of attack of 12.9°. Again it should be pointed out that a greater number of pressure orifices located in the immediate vicinity of the leading edge may have led to pressure readings which would have indicated pressures as high as or higher than the critical pressure coefficient. Such a condition could lead to the possibility of slight shock disturbances having an influence on the leading-edge separation. Because a turbulent boundary layer probably forms closely behind the leading-edge separation point, the flow reattaches to the upper surface a short distance in back of the separation point. However, the adverse effect of the leading-edge separation probably causes the turbulent boundary layer in back of the separated region to thicken until finally separation occurs over the trailing edge. (See reference 13.) The stall first began near the midsemispan station and then spread out to cover the rest of the wing. (See fig. 13.)

A study of the pressure distributions for Mach numbers of 0.25 to 0.35 (which are not presented) indicated that the stall at these Mach numbers was also associated with both leading-edge and trailing-edge separation. With increasing Mach number, however, these pressure distributions showed that the effect of trailing-edge separation became relatively more important than the effect of leading-edge separation.

The moderate-speed stall (figs. 12(b) and 14) differs appreciably from the low-speed stall. The moderate-speed stall occurs gradually with increasing angle of attack and appears to be due to separation gradually moving forward from the trailing edge. No apparent leading-edge separation takes place at this Mach number because turbulence probably forms close to the leading edge and prevents the occurrence of laminar separation behind the peak pressure points. The stall first appeared at about the midsemispan station and then spread slowly over the rest of the wing. (See fig. 14.)

The high-speed stall (figs. 12(c) and 15) also was associated with trailing-edge separation but it occurred abruptly along with a simultaneous breakdown of the large region of supersonic flow formed over the forward part of the upper surface. The large region of supersonic flow formed for this Mach number condition ($M_o = 0.60$) increased until it extended over approximately 30 percent of the chord and had a peak local Mach number of approximately 1.78 at maximum normal force. These maximum conditions occurred at the midsemispan station for an angle of attack

of 12.0°. (See fig. 12(c).) Figure 15 shows that although all sections showed signs of stalling at approximately the same angle of attack, the effects of the stall were most severe at the midsemispan station.

Span-Load Distributions

Figure 16 presents a comparison between experimental and calculated span-load distributions for Mach numbers of 0.20, 0.40, and 0.60. Although the calculated span-load distributions (which were determined by the method of reference 15) are based on low-speed data, good agreement with the experimental span-load distributions is shown for all the Mach number conditions presented in figure 16. However, a comparison between the low-speed and high-speed experimental span-load distributions does indicate that there is a slight inboard shift in the center of normal force at high speeds.

As can be seen in figure 17, the effect of Mach number on the inboard shift of lateral center of normal force is very slight. The comparison made between experimental and calculated lateral centers of normal force in figure 17 shows excellent agreement, the difference being always less than 1 percent of the semispan for normal-force coefficients varying from 0.20 to the maximum. Above the angle of attack at which the maximum normal-force coefficient occurs there is a sudden outboard shift of the lateral center of normal force, the largest shift being at a Mach number of 0.40 for the three Mach number conditions shown.

Section Pitching-Moment Distribution

The spanwise variation of section pitching-moment parameter with normal-force coefficient is shown in figure 18 for Mach numbers of 0.20, 0.40, and 0.60. These pitching-moment distributions illustrate the effect on section pitching-moment parameters of large pressures near the leading edge at the root sections and of large moment arms at the outer wing sections.

Below the stall range, the greatest difference existing between the pitching-moment distributions for various Mach numbers is that, over the inboard sections, larger positive increases in the section pitching-moment parameters occur at the higher normal-force coefficients for a Mach number of 0.60 (fig. 18(c)) than at lower speeds. These larger increases are due to large forward shifts in center of pressure that are caused by extensive regions of supersonic flow over the forward part of the upper surface.

Pitching-Moment Coefficient

The effect of Mach number on the variation of pitching-moment coefficient with angle of attack is presented in figure 19. For low angles of attack, the change caused in pitching-moment coefficient from a Mach number of 0.20 to a Mach number of 0.60 by the effect of Mach number agrees closely with that predicted by the Glauert factor $\frac{1}{\sqrt{1 - M_o^2}}$. Although this factor underestimates the change from a Mach number of 0.20 to a Mach number of 0.40 by about 50 percent, the change is probably within experimental accuracy.

At the higher angles of attack the pitching-moment curve for a Mach number of 0.60 shows a decrease in longitudinal stability because the center of pressure moves forward owing to the formation of large regions of supersonic flow over the forward part of the upper surface.

SUMMARY OF RESULTS

Results of a wind-tunnel investigation at Mach numbers up to 0.60 of a tapered wing having NACA 64-210 airfoil sections and an aspect ratio of 6 indicated the following:

1. The maximum lift coefficient increased from a value of 1.02 at a Mach number of 0.15 to a low-speed peak value of 1.05 at a Mach number of 0.20; decreased to a value of 0.95 at a Mach number of 0.40; and then increased slowly to a value of 1.00 at a Mach number of 0.55, after which it increased rapidly to a value of 1.09 at a Mach number of 0.60 (limit of maximum-lift tests).

2. Maximum lift at Mach numbers between 0.40 and 0.55 was attained at angles of attack appreciably greater than those at which stalling first became apparent. The angle-of-attack difference was about 10° at Mach numbers of 0.45 and 0.50.

3. At the higher Mach numbers and angles of attack for an unstalled condition, extensive regions of supersonic flow were formed over the forward part of the upper surface and resulted in large increases in lift coefficient; a peak local Mach number of about 1.78 was obtained at a free-stream Mach number of 0.60 and an angle of attack of 12.0°.

4. The low-speed stall (Mach number of 0.20) occurred rapidly and was characterized by a combination of leading-edge and trailing-edge separations; whereas the moderate-speed stall (Mach number of 0.40) which occurred gradually and the high-speed stall (Mach number of 0.60) which occurred rapidly were associated with trailing-edge separation.

5. Longitudinal stability decreased at the higher angles of attack and Mach numbers because the center of pressure moved forward with the occurrence of large regions of supersonic flow over the forward part of the upper surface.

6. Mach number had only a slight effect on span-load distributions and on the shift of lateral center of normal force for angles of attack below the stall.

Langley Aeronautical Laboratory
National Advisory Committee for Aeronautics
Langley Air Force Base, Va., February 25, 1949

REFERENCES

1. Muse, Thomas C.: Some Effects of Reynolds and Mach Numbers on the Lift of an NACA 0012 Rectangular Wing in the NACA 19-Foot Pressure Tunnel. NACA CB No. 3E29, 1943.

2. Cleary, Harold E.: Effects of Compressibility on Maximum Lift Coefficients for Six Propeller Airfoils. NACA ACR No. L4L21a, 1945.

3. Nissen, James M., and Gadeberg, Burnett L.: Effect of Mach and Reynolds Numbers on the Power-Off Maximum Lift Coefficient Obtainable on a P-39N-1 Airplane as Determined in Flight. NACA ACR No. 4F28, 1944.

4. Rhode, Richard V.: Correlation of Flight Data on Limit Pressure Coefficients and Their Relation to High-Speed Burbling and Critical Tail Loads. NACA ACR No. L4I27, 1944.

5. Pearson, E. O., Jr., Evans, A. J., and West, F. E., Jr.: Effects of Compressibility on the Maximum Lift Characteristics and Spanwise Load Distribution of a 12-Foot-Span Fighter-Type Wing of NACA 230-Series Airfoil Sections. NACA ACR No. L5G10, 1945.

6. Pearson, E. O., Jr.: Effect of Compressibility on the Distribution of Pressures over a Tapered Wing of NACA 230-Series Airfoil Sections. NACA TN No. 1390, 1947.

7. Furlong, G. Chester, and Fitzpatrick, James E.: Effects of Mach Number and Reynolds Number on the Maximum Lift Coefficient of a Wing of NACA 230-Series Airfoil Sections. NACA TN No. 1299, 1947.

8. Cooper, Morton, and Korycinski, Peter F.: The Effects of Compressibility on the Lift, Pressure, and Load Characteristics of a Tapered Wing of NACA 66-Series Airfoil Sections. NACA TN No. 1697, 1948.

9. Wall, Nancy E.: Chordwise Pressure Distributions on a 12-Foot-Span Wing of NACA 66-Series Airfoil Sections up to a Mach Number of 0.60. NACA TN No. 1696, 1948.

10. West, F. E., Jr., and Hallissy, J. M., Jr.: Effects of Compressibility on Normal-Force, Pressure, and Load Characteristics of a Tapered Wing of NACA 66-Series Airfoil Sections with Split Flaps. NACA TN No. 1759, 1948.

11. Abbott, Ira H., Von Doenhoff, Albert E., and Stivers, Louis S., Jr.: Summary of Airfoil Data. NACA Rep. No. 824, 1945.

12. Göthert, B.: Plane and Three-Dimensional Flow at High Subsonic Speeds. NACA TM No. 1105, 1946.

13. Jacobs, Eastman N., and Sherman, Albert: Airfoil Section Characteristics as Affected by Variations of the Reynolds Number. NACA Rep. No. 586, 1937.

14. Stack, John, Fedziuk, Henry A., and Cleary, Harold E.: Preliminary Investigation of the Effect of Compressibility on the Maximum Lift Coefficient. NACA ACR, Feb. 1943.

15. Anon.: Spanwise Air-Load Distribution. ANC-1(1), Army-Navy-Commerce Committee on Aircraft Requirements. U. S. Govt. Printing Office, April 1938.

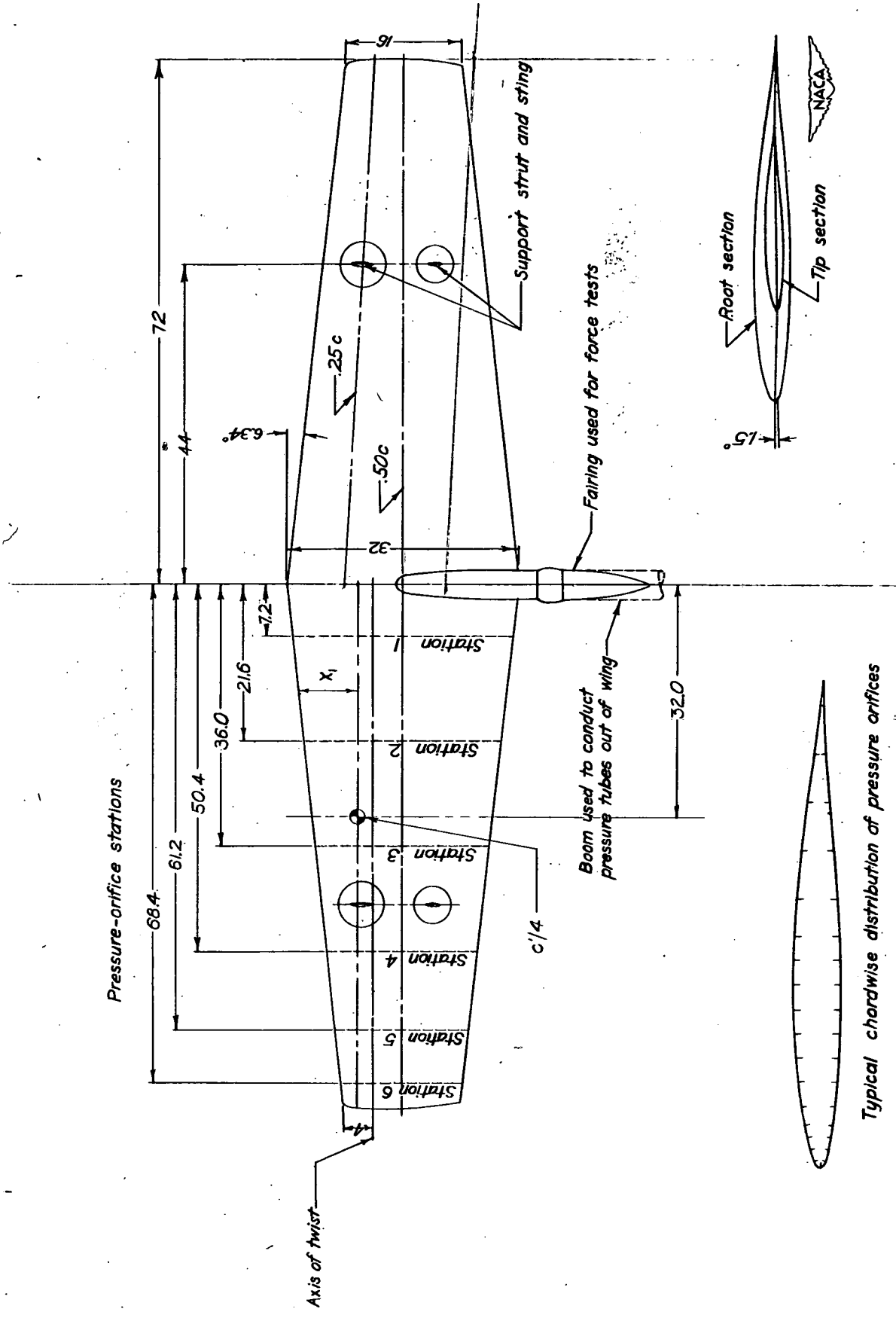

Figure 1.– Principal wing dimensions and location of pressure orifices. (All dimensions are in inches.)

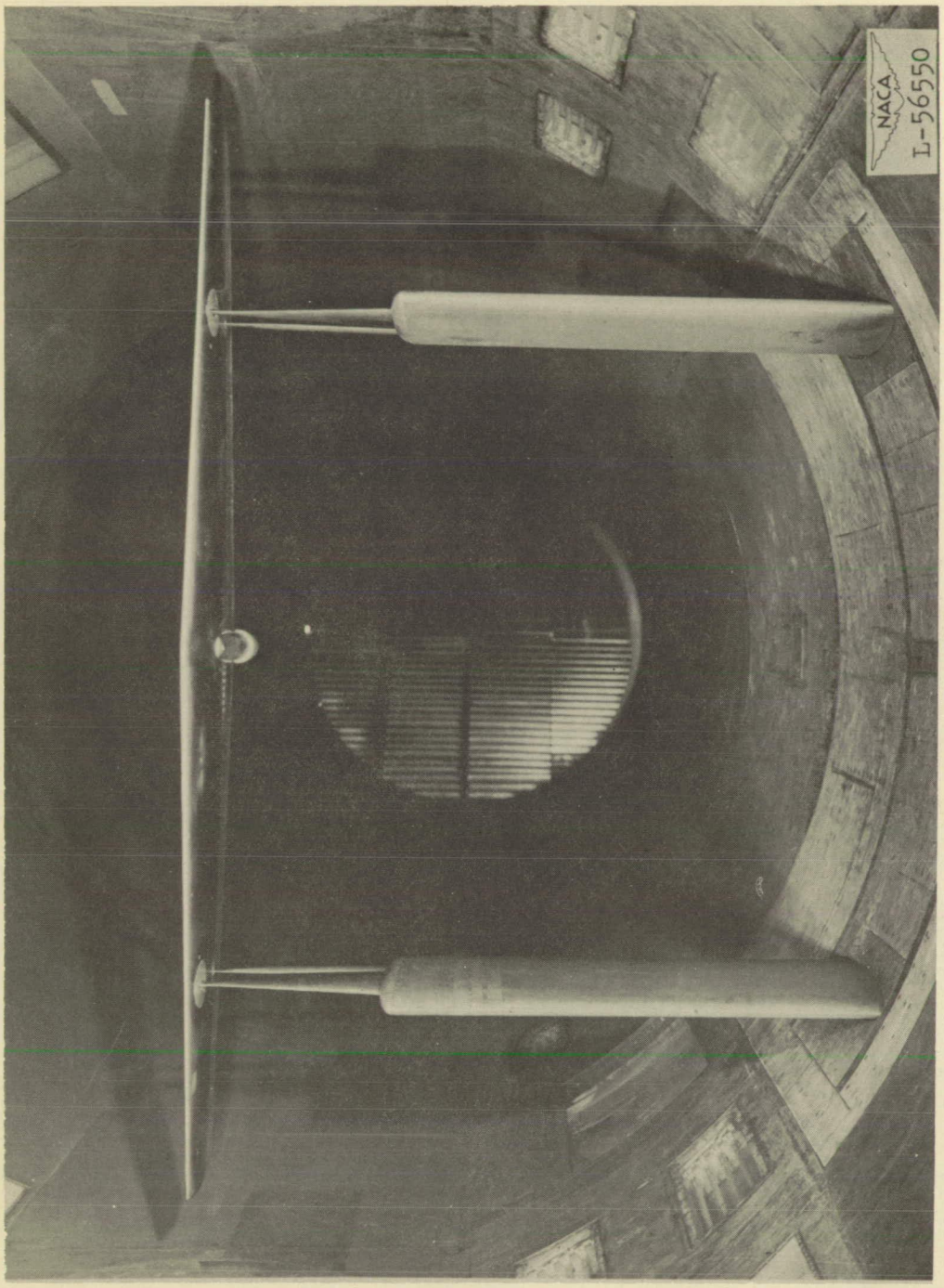

Figure 2.- Front view of wing showing basic-force-test installation.

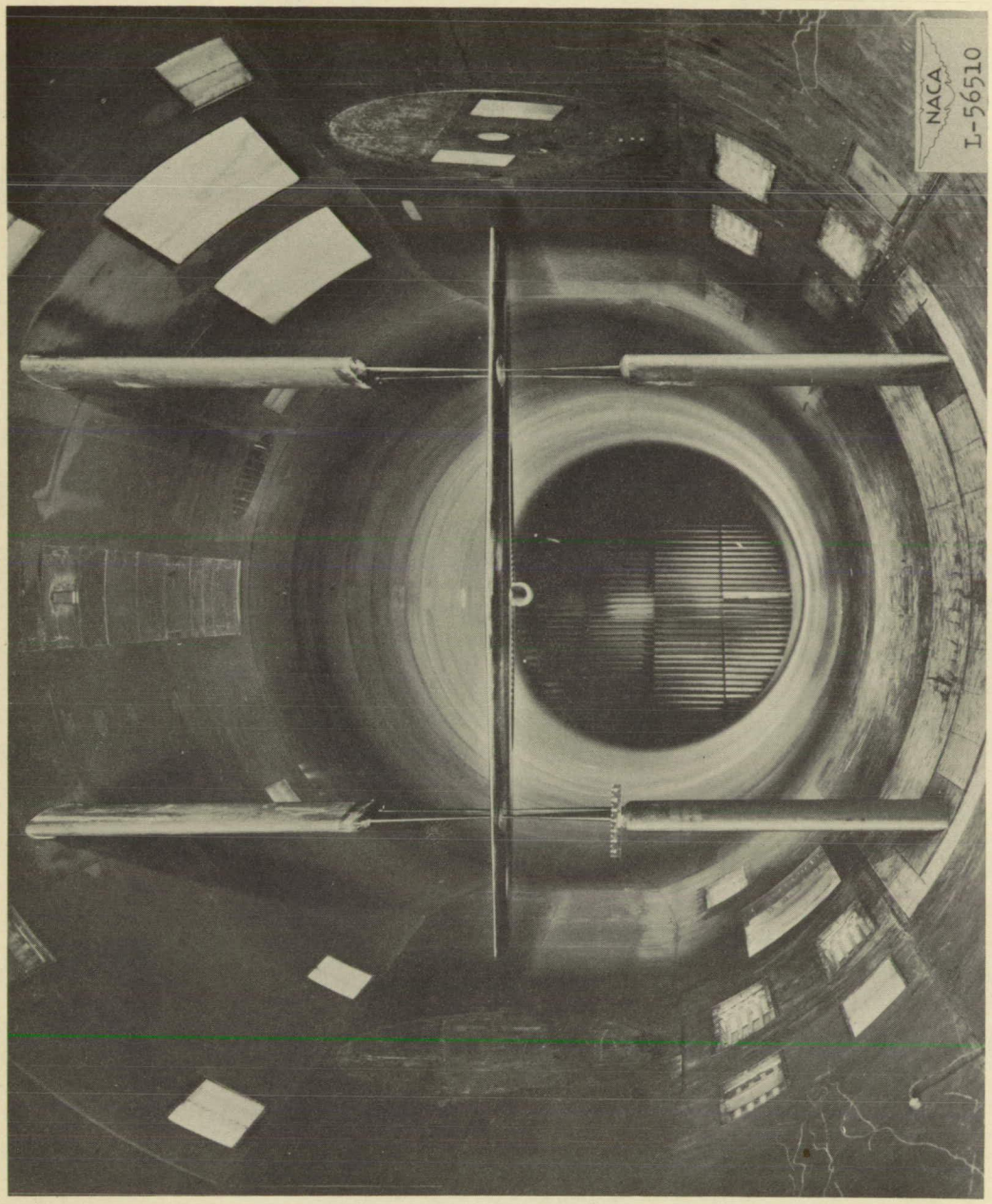

Figure 3.- Front view of wing with image struts installed for the determination of force tare corrections.

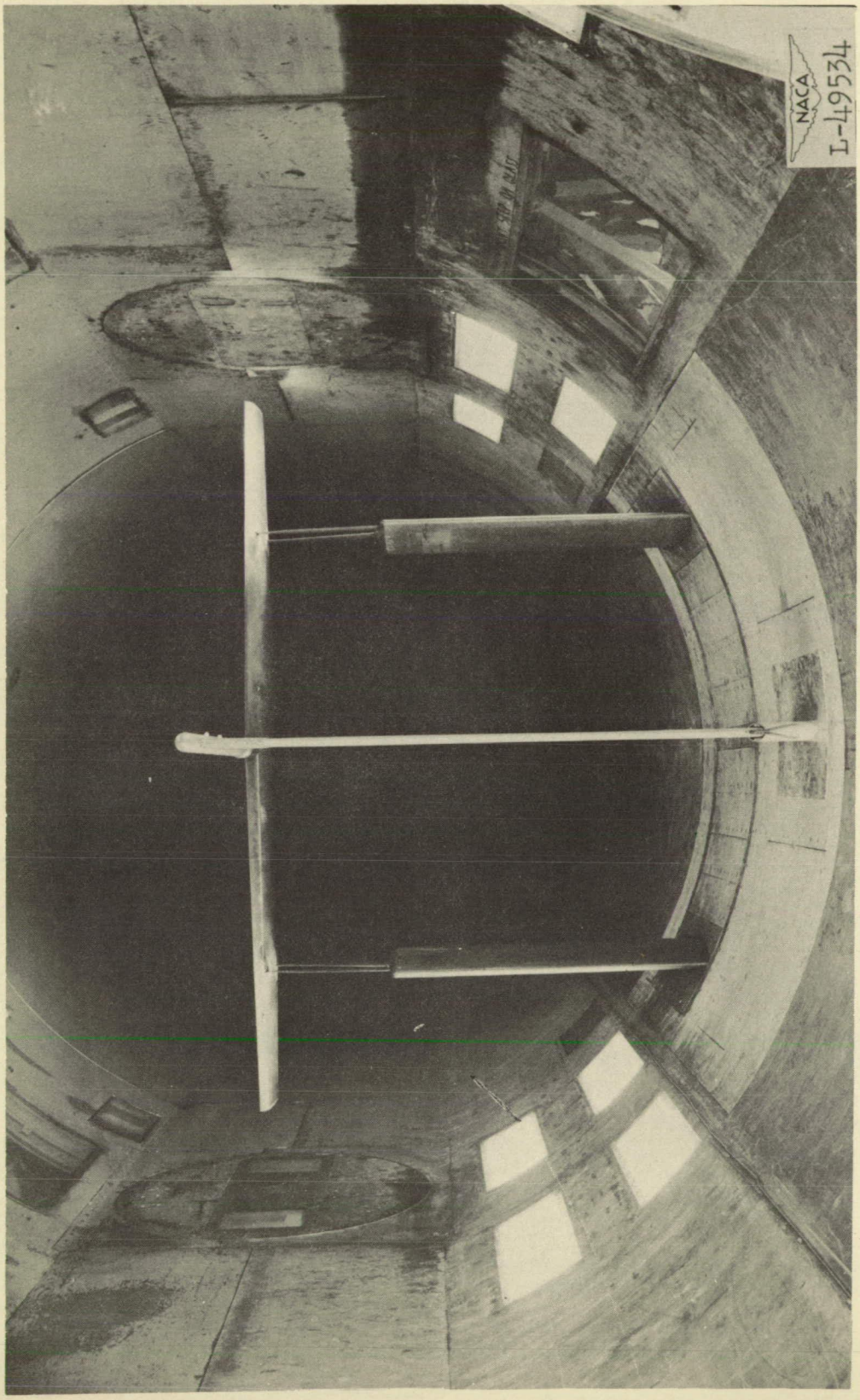

Figure 4.- Rear view of wing showing pressure-test installation.

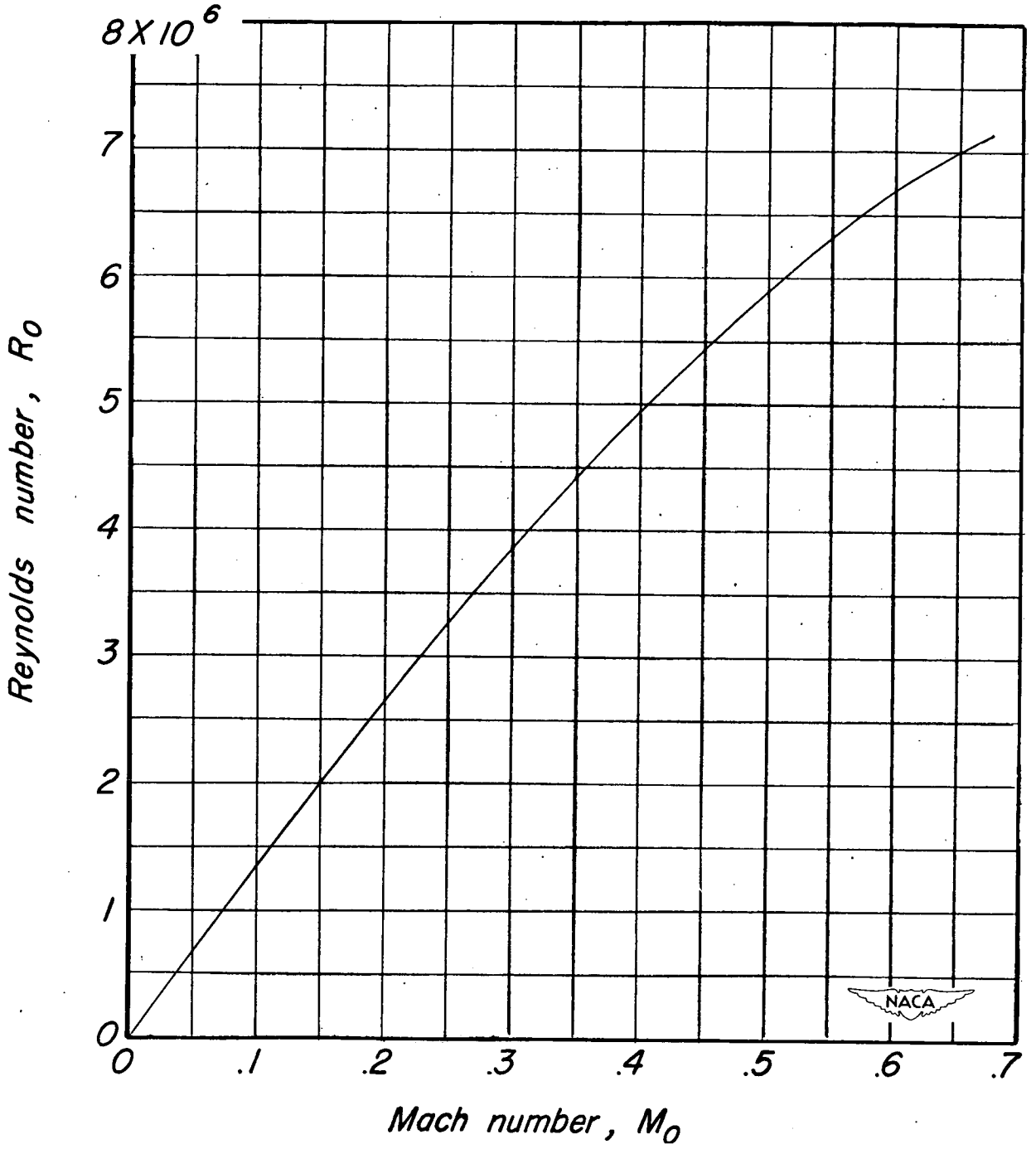

Figure 5.– Variation of average test Reynolds number with Mach number.

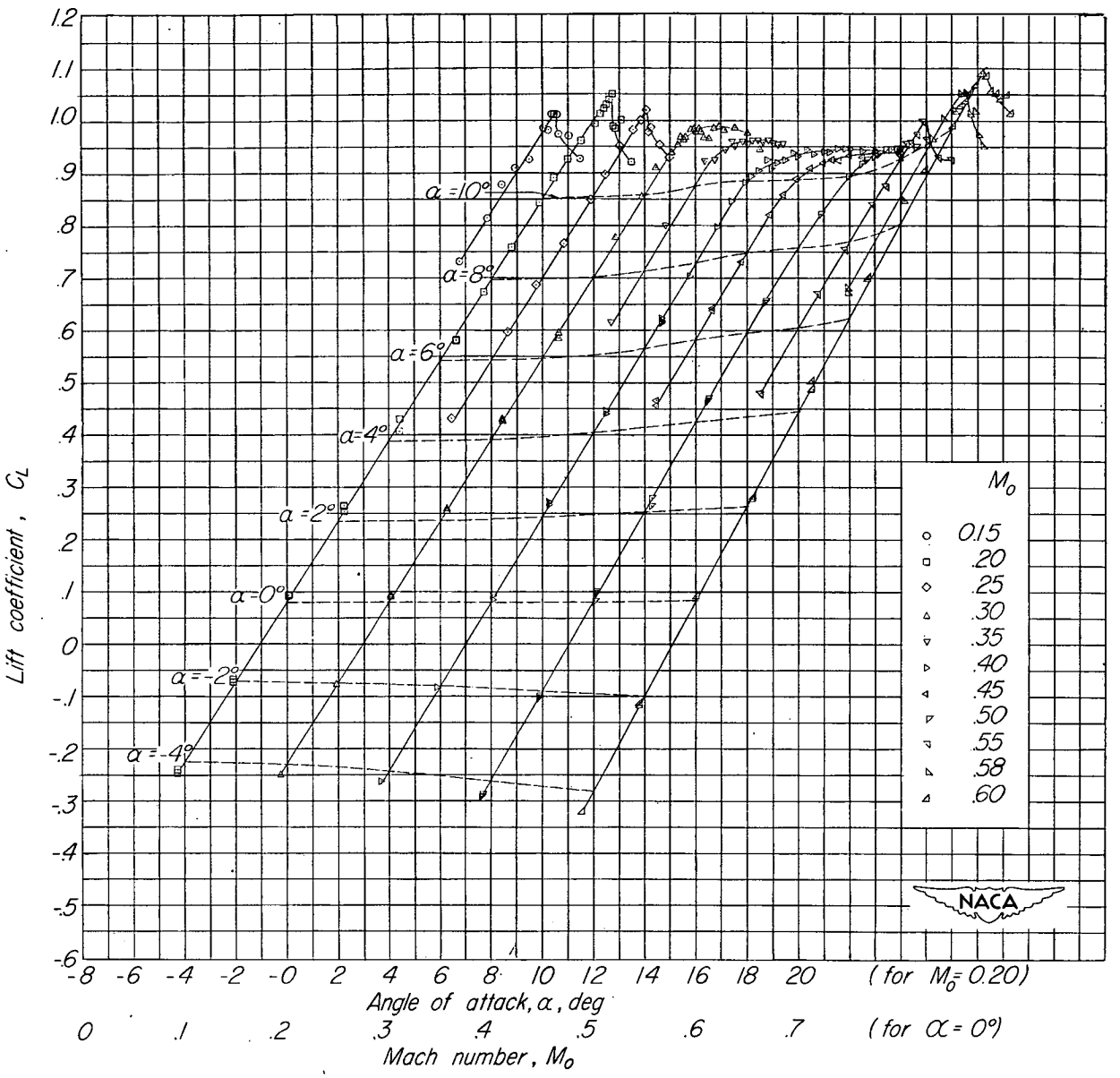

Figure 6.– Lift coefficient as a function of angle of attack and Mach number.

ENGINEERING DEPT. LIBRARY
CHANCE-VOUGHT AIRCRAFT
DALLAS, TEXAS

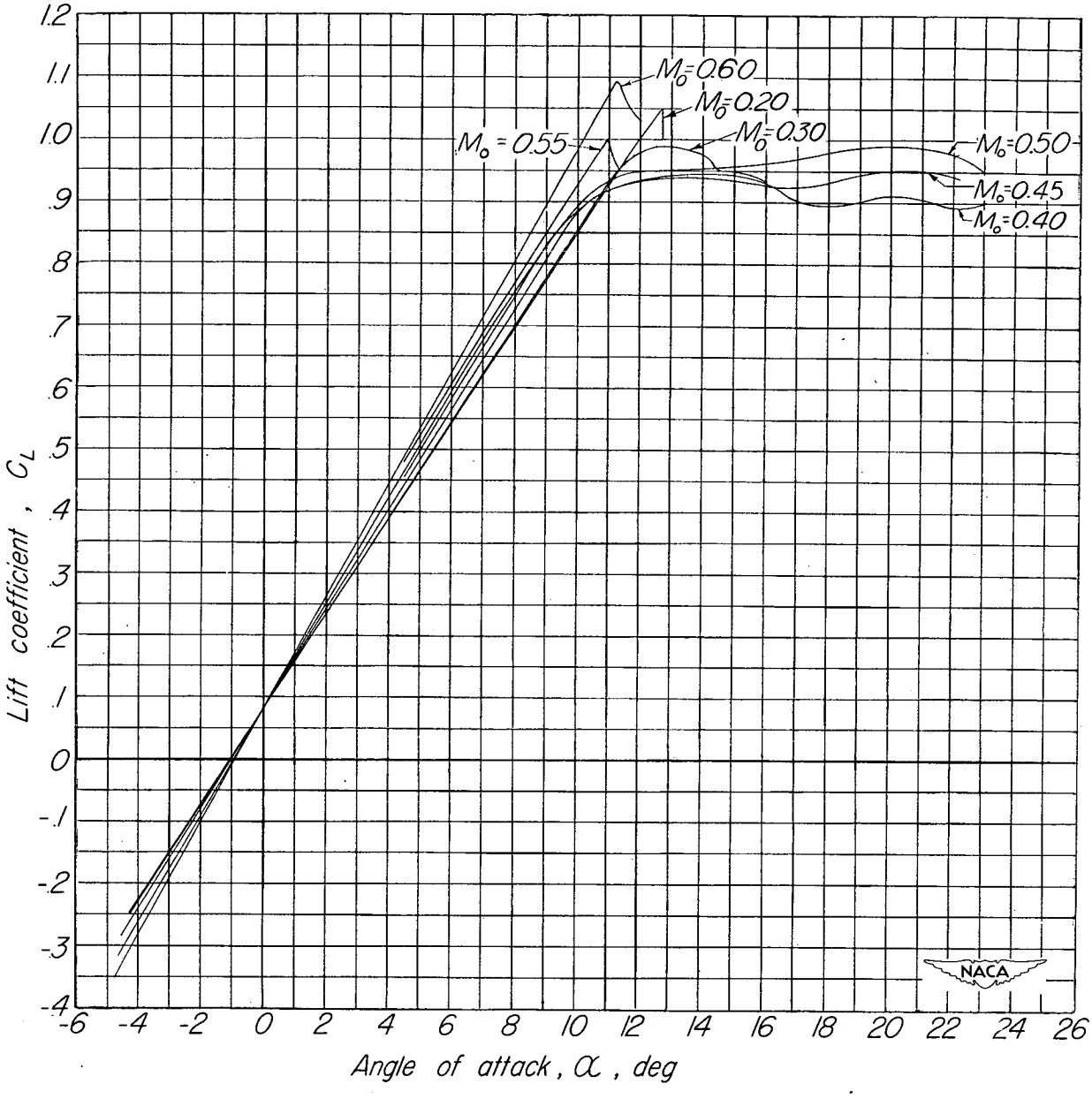

Figure 7.– Variation of lift coefficient with angle of attack for several Mach numbers.

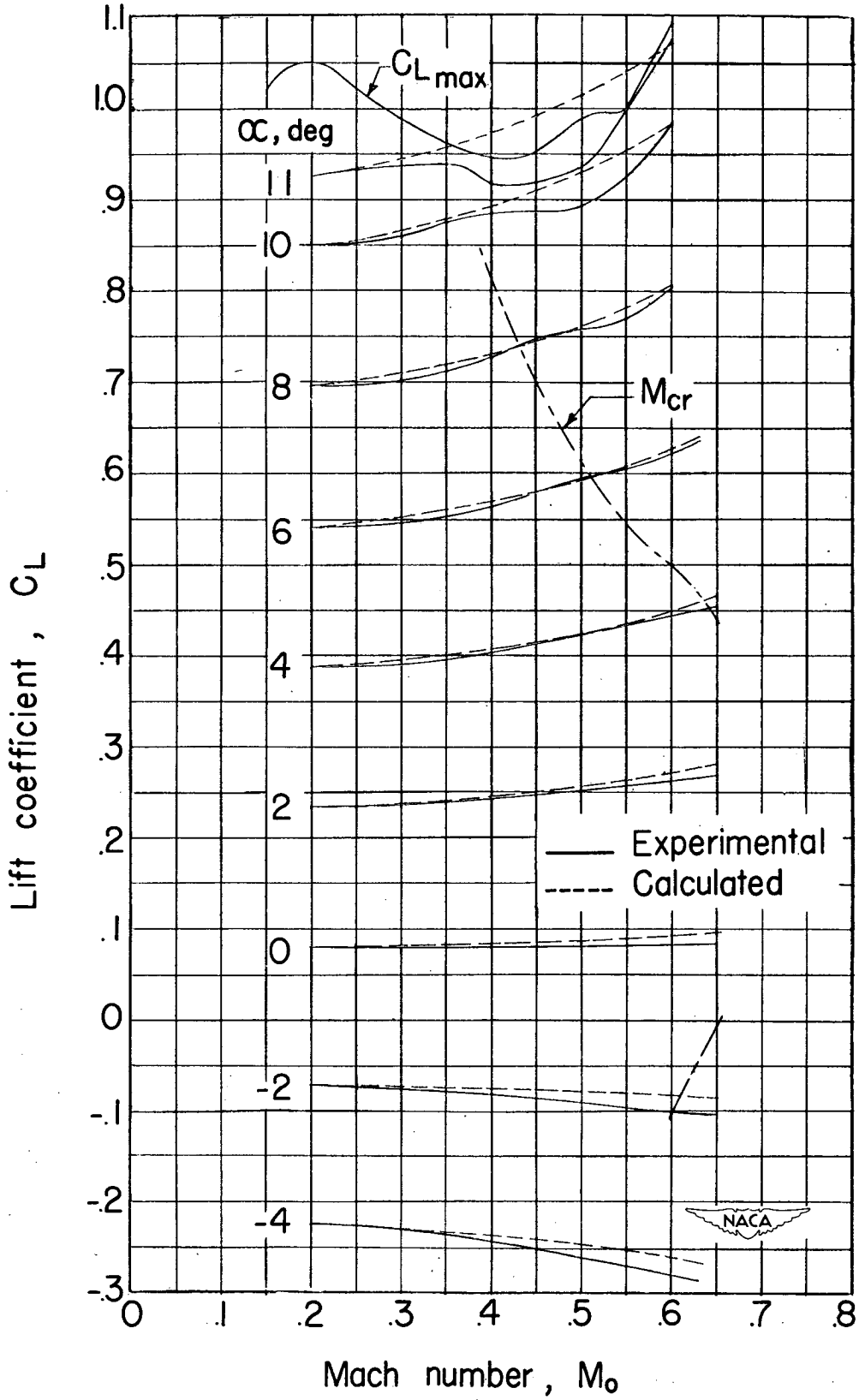

Figure 8.– Variation of experimental and calculated lift coefficients with Mach number for several angles of attack.

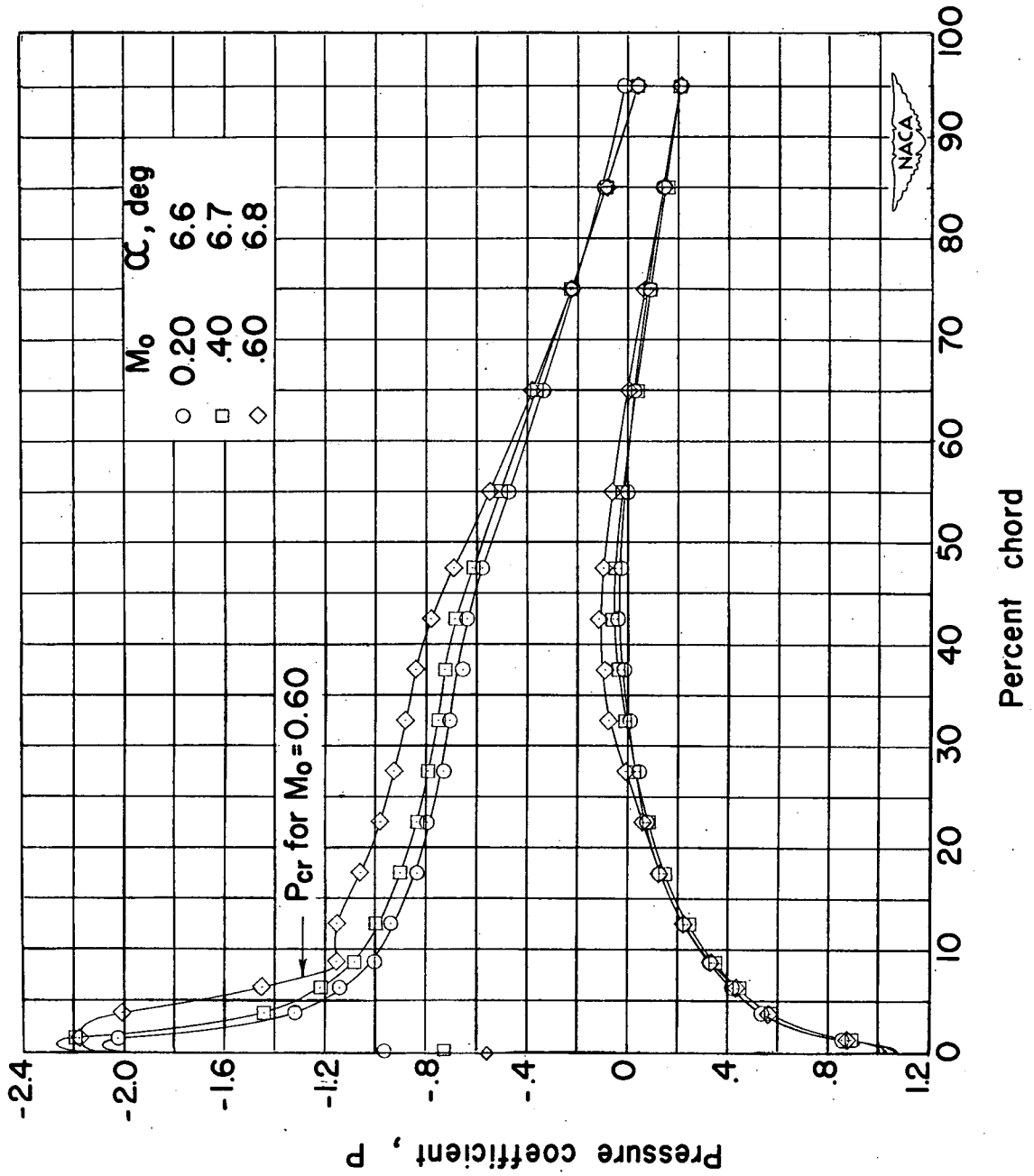

Figure 9.- Effect of Mach number on the pressure distribution at station 3 for an angle of attack of about 6.7°.

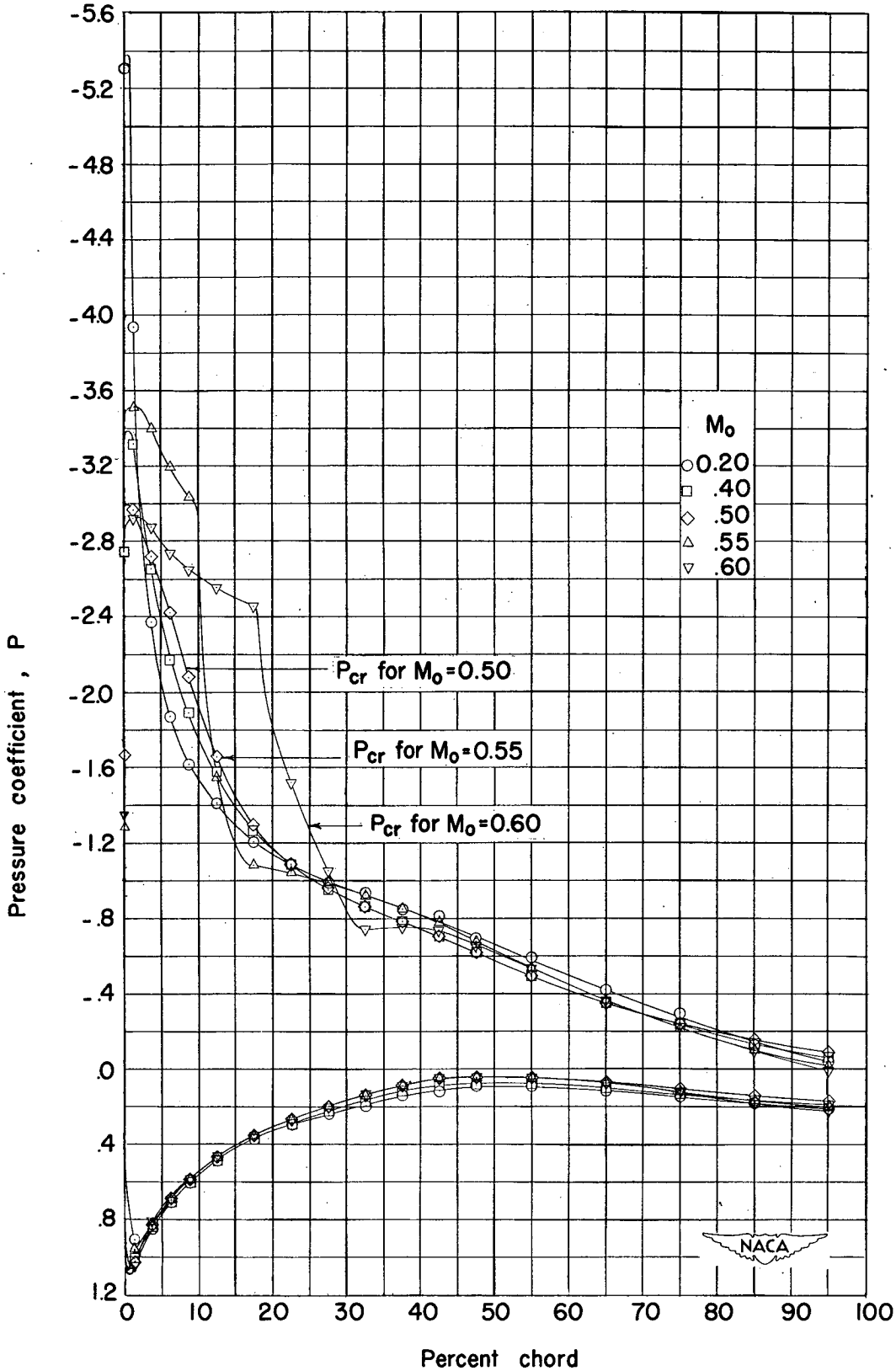

Figure 10.– Effect of Mach number on the pressure distribution at station 3 for an angle of attack of 11.0°.

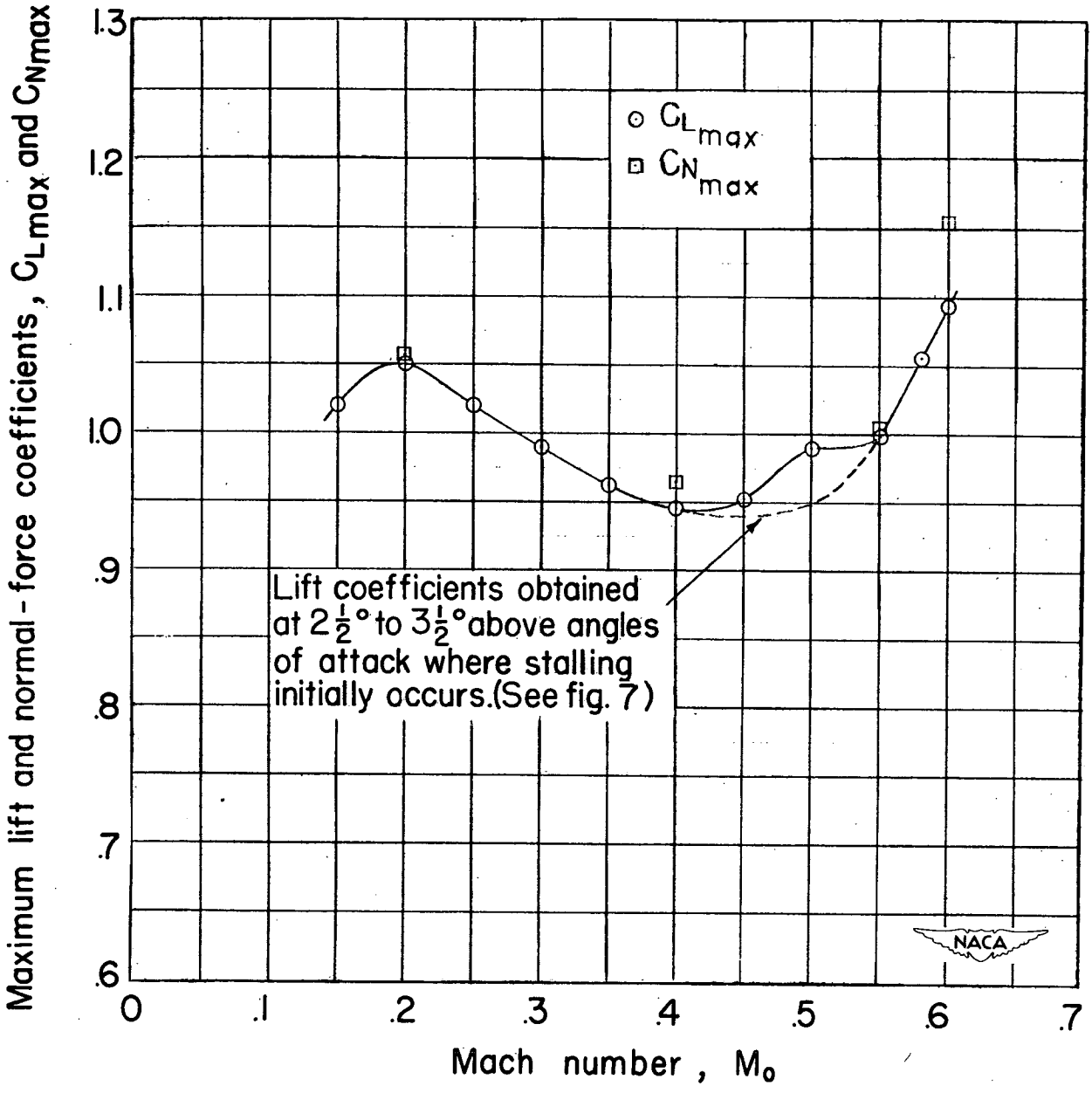

Figure 11.– Variation of maximum lift coefficient with Mach number.

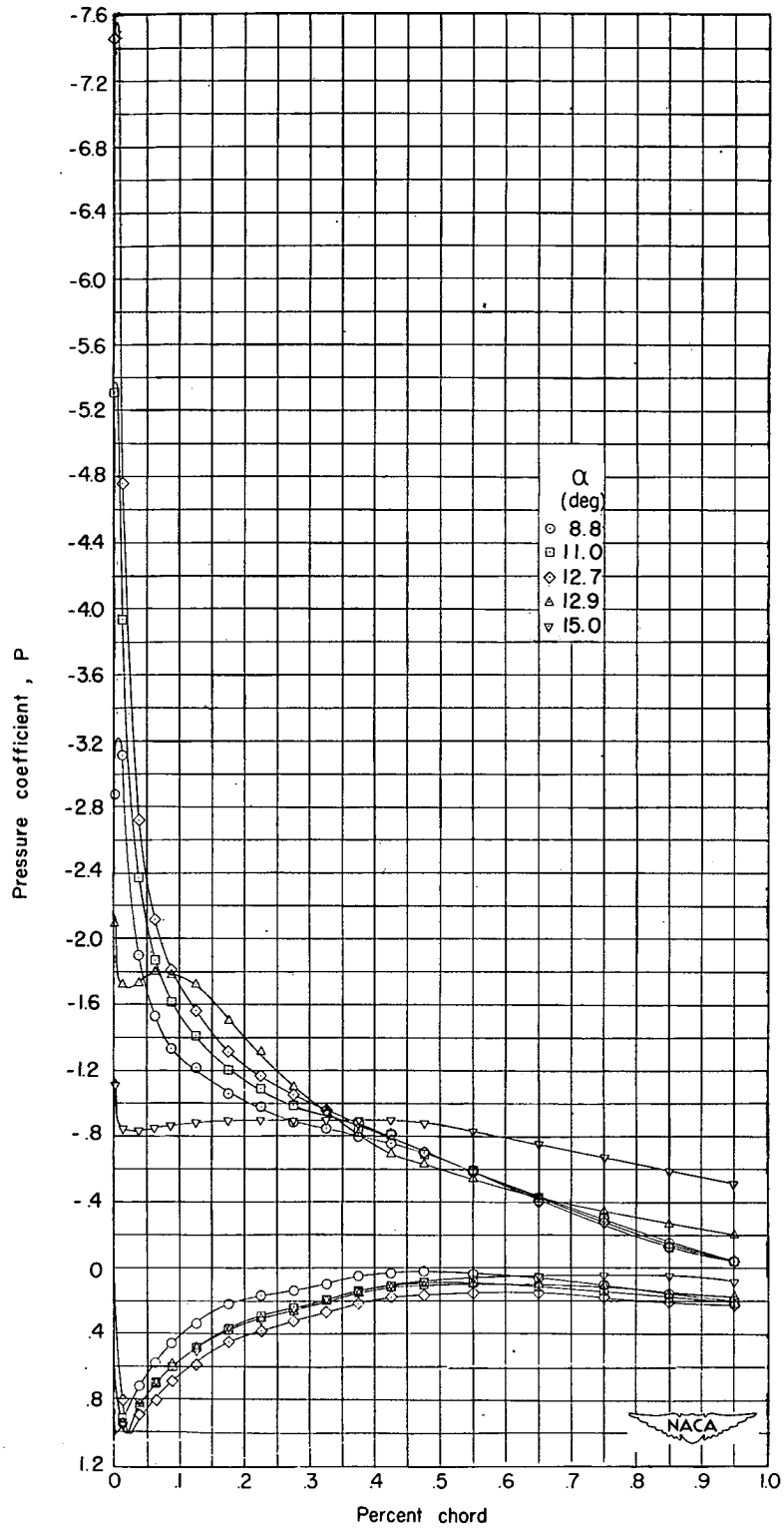

(a) $M_o = 0.20$.

Figure 12.– Variation of the pressure distribution at station 3 with angle of attack for several Mach numbers.

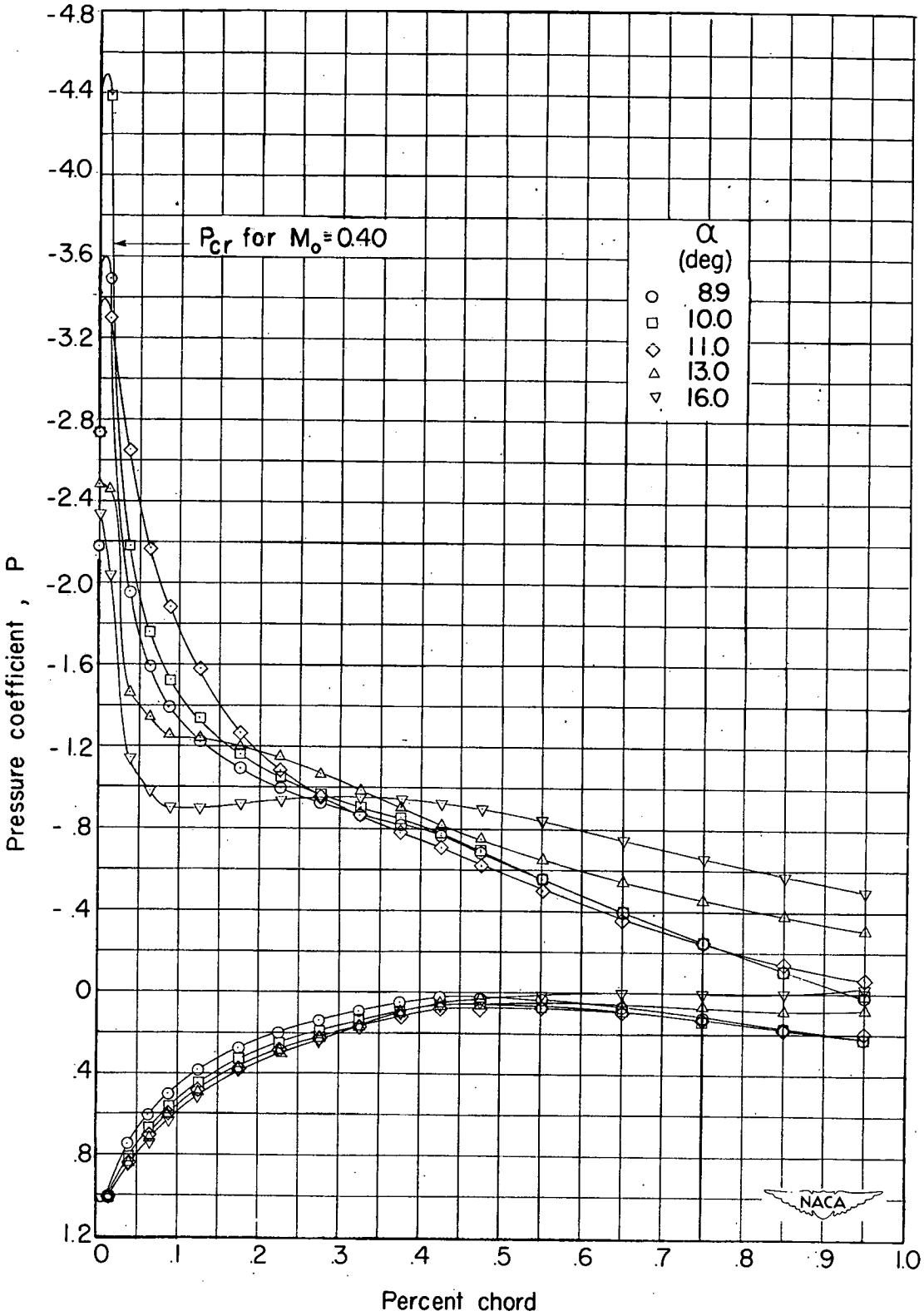

(b) M_o = 0.40.

Figure 12.– Continued.

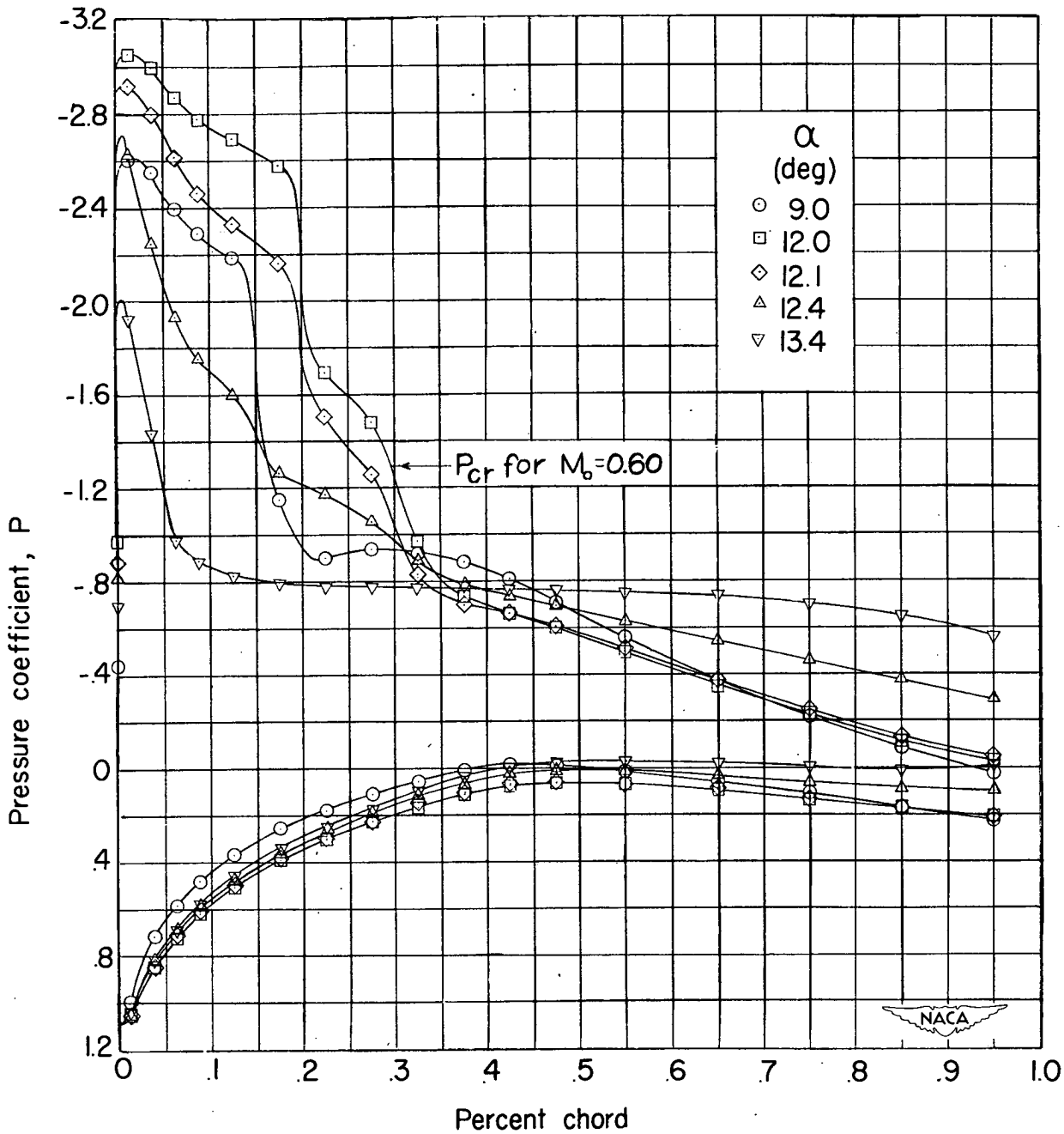

(c) M_o = 0.60.

Figure 12.– Concluded.

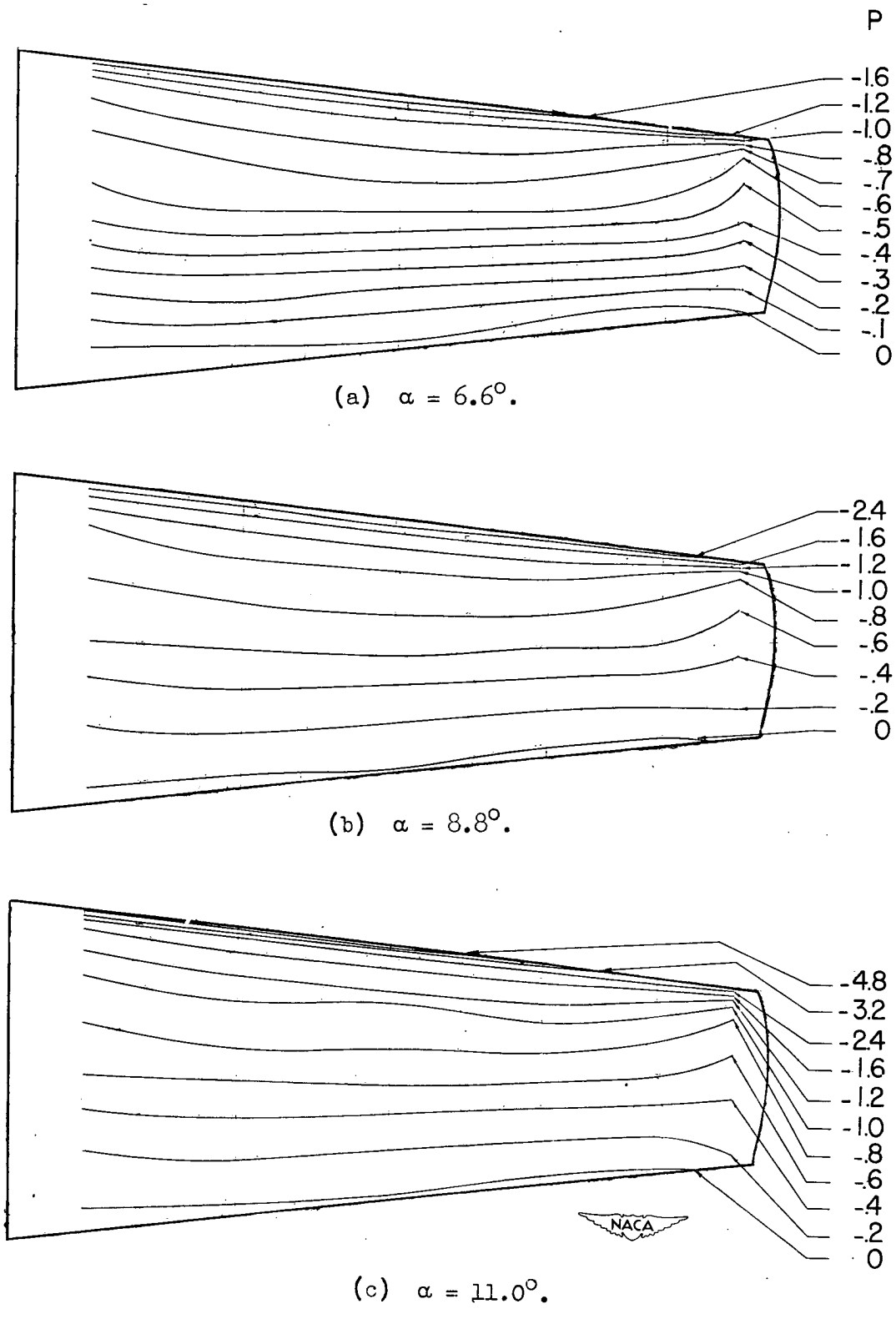

Figure 13.– Pressure contours over the upper surface for several angles of attack at a Mach number of 0.20.

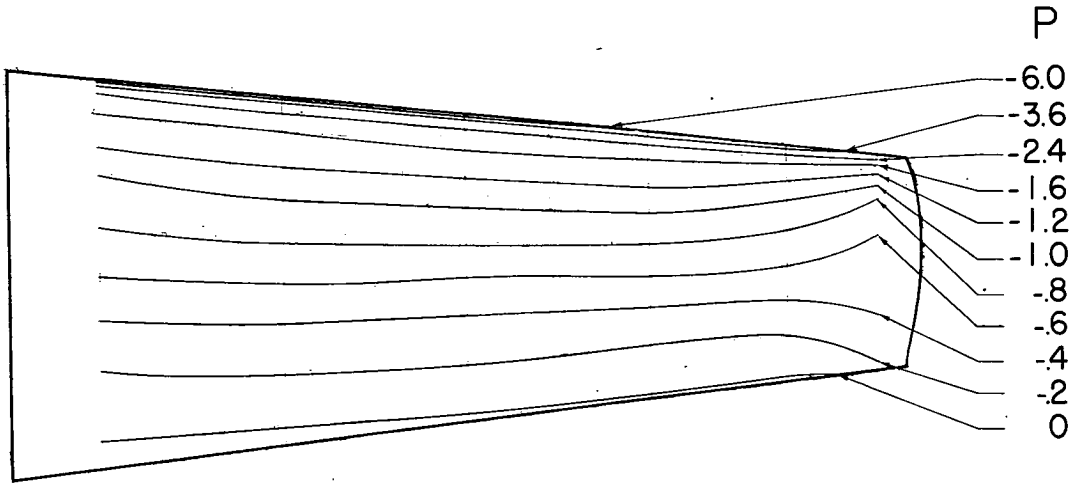

(d) $\alpha = 12.7^{\circ}$.

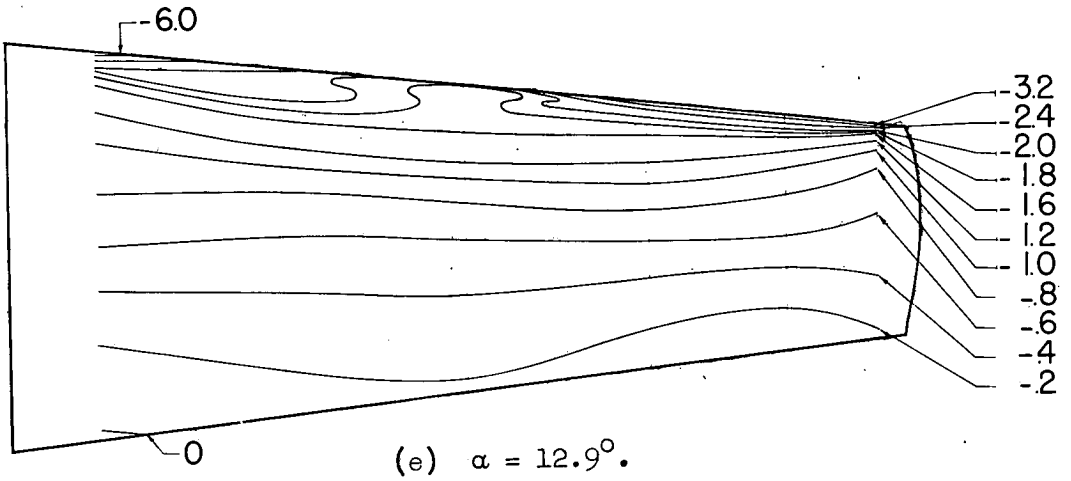

(e) $\alpha = 12.9^{\circ}$.

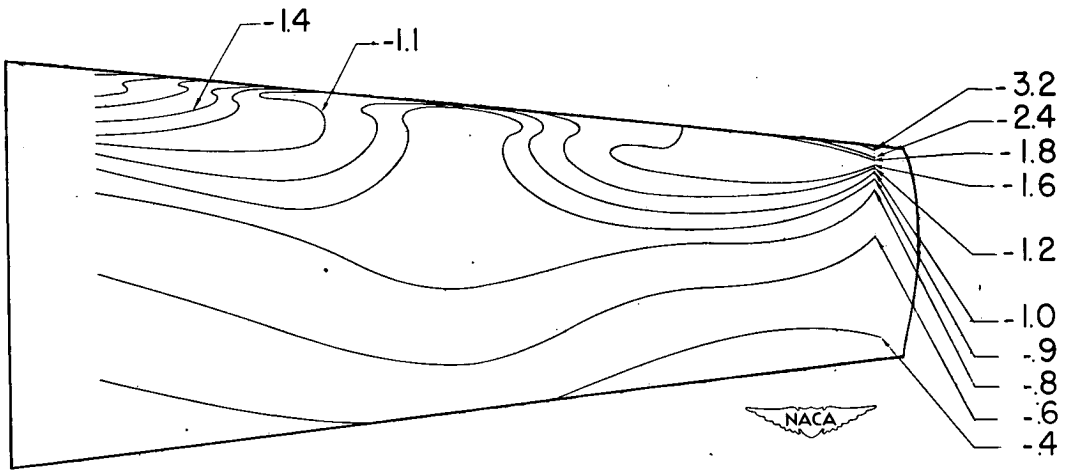

(f) $\alpha = 15^{\circ}$.

Figure 13.– Concluded.

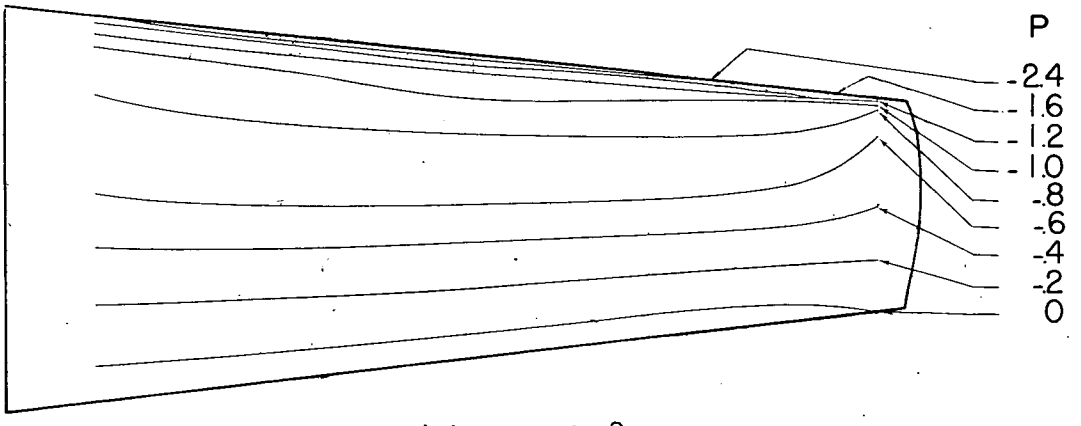

(a) $\alpha = 6.7^{\circ}$.

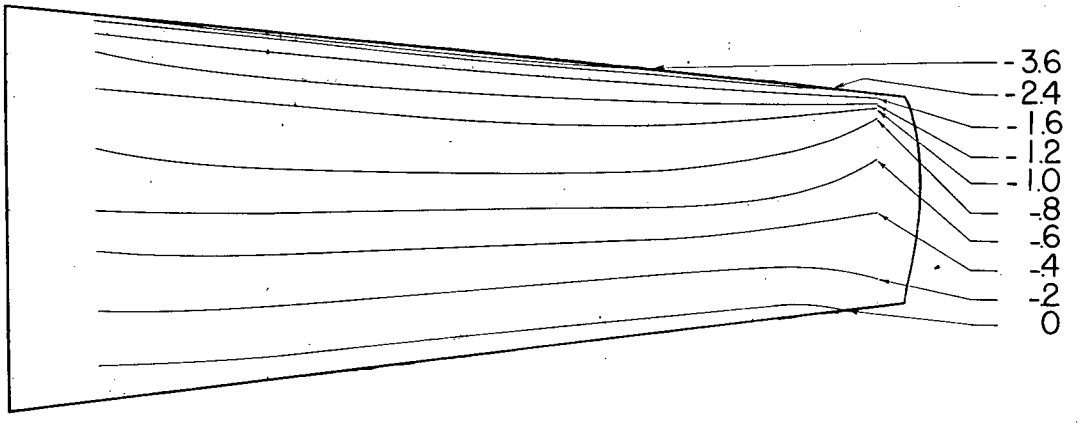

(b) $\alpha = 8.9^{\circ}$.

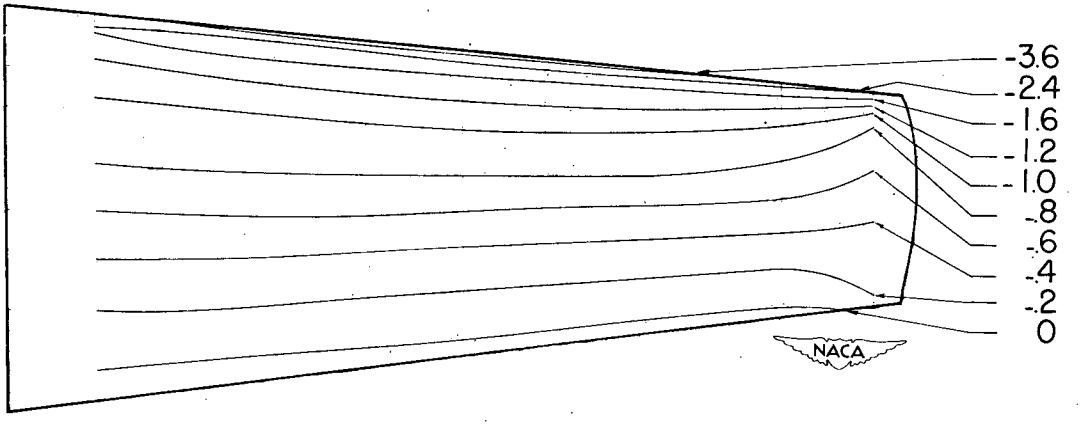

(c) $\alpha = 10.0^{\circ}$.

Figure 14.– Pressure contours over the upper surface for several angles of attack at a Mach number of 0.40.

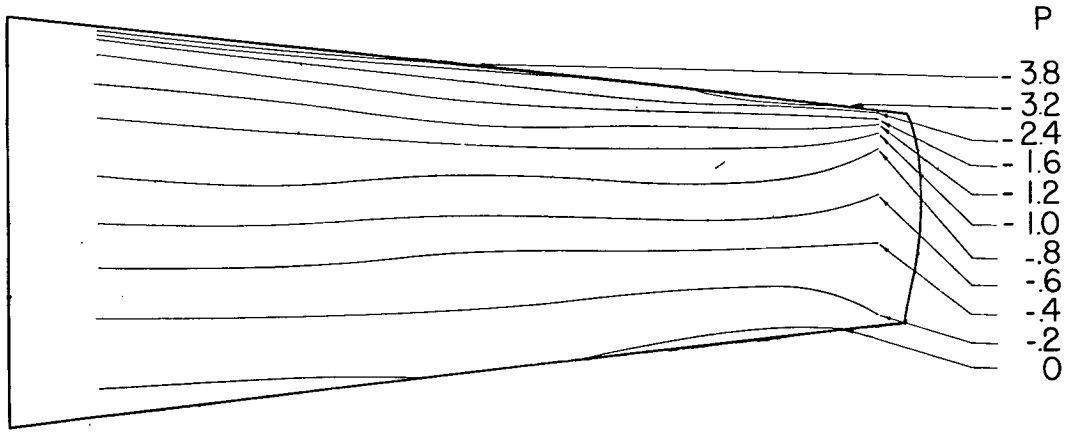

(d) $\alpha = 11^{\circ}$.

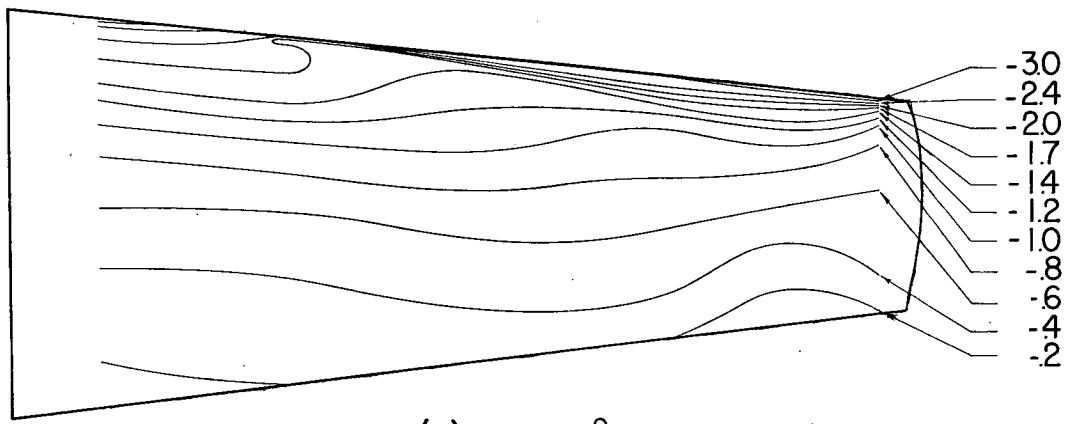

(e) $\alpha = 13^{\circ}$.

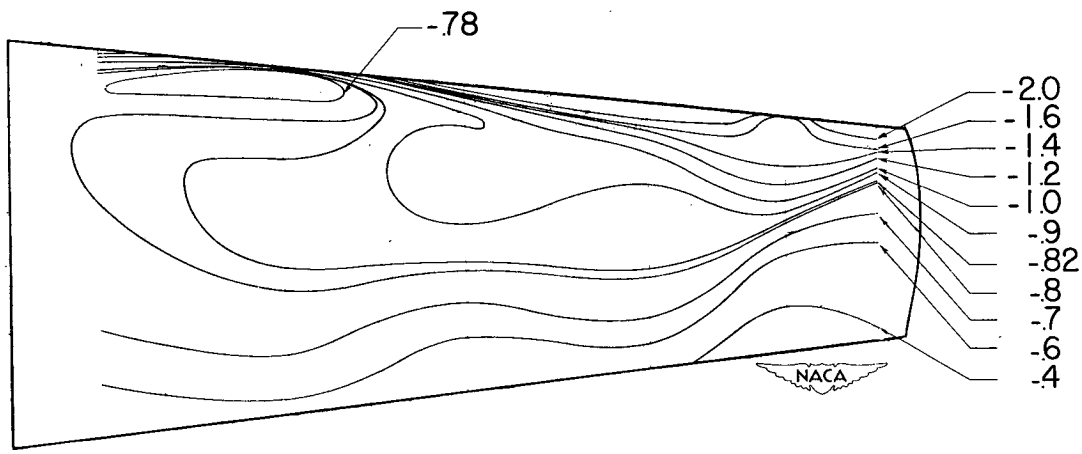

(f) $\alpha = 16^{\circ}$.

Figure 14.– Concluded.

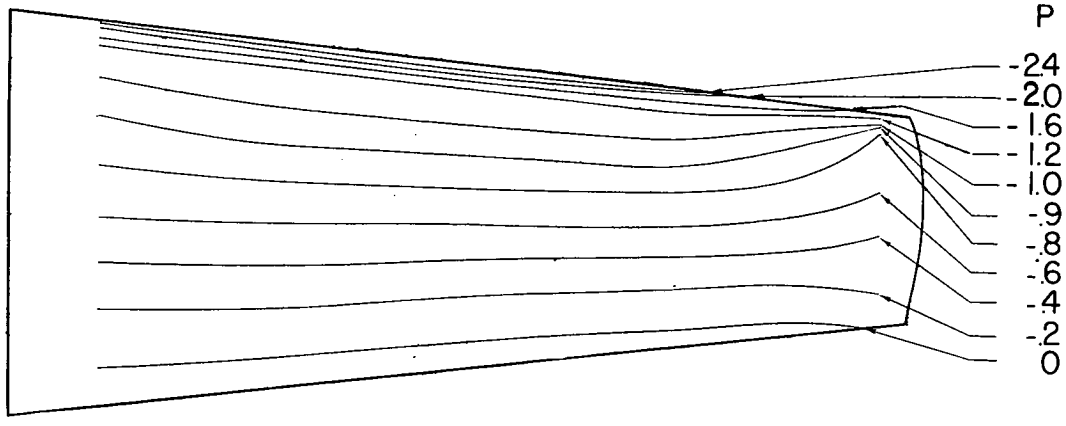

(a) $\alpha = 6.8^{\circ}$.

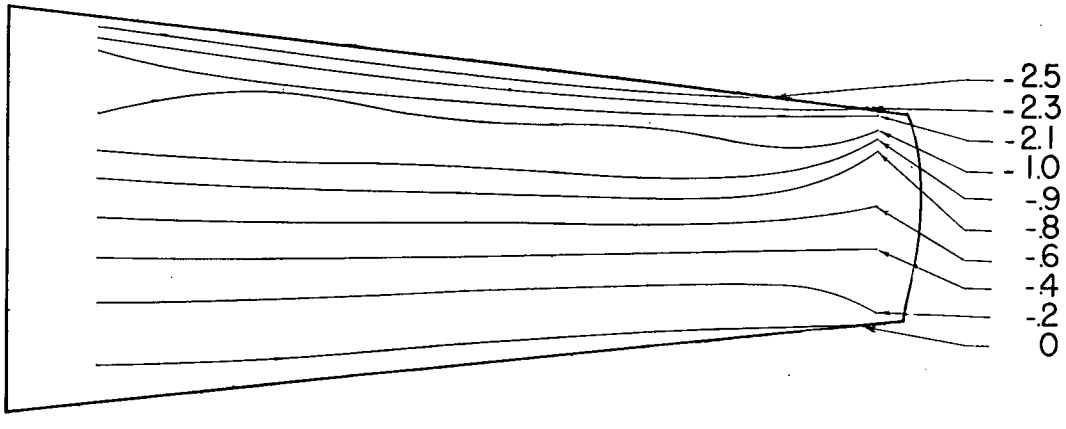

(b) $\alpha = 9^{\circ}$.

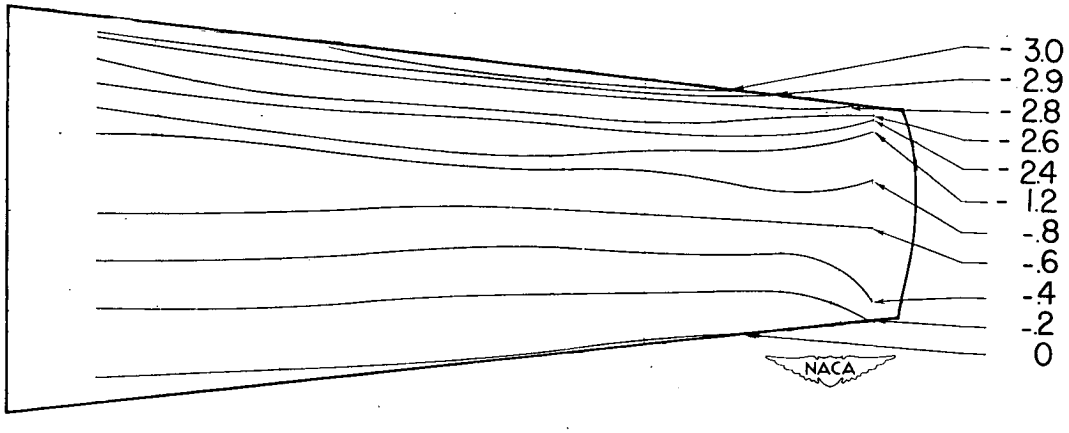

(c) $\alpha = 12^{\circ}$.

Figure 15.– Pressure contours over the upper surface for several angles of attack at a Mach number of 0.60.

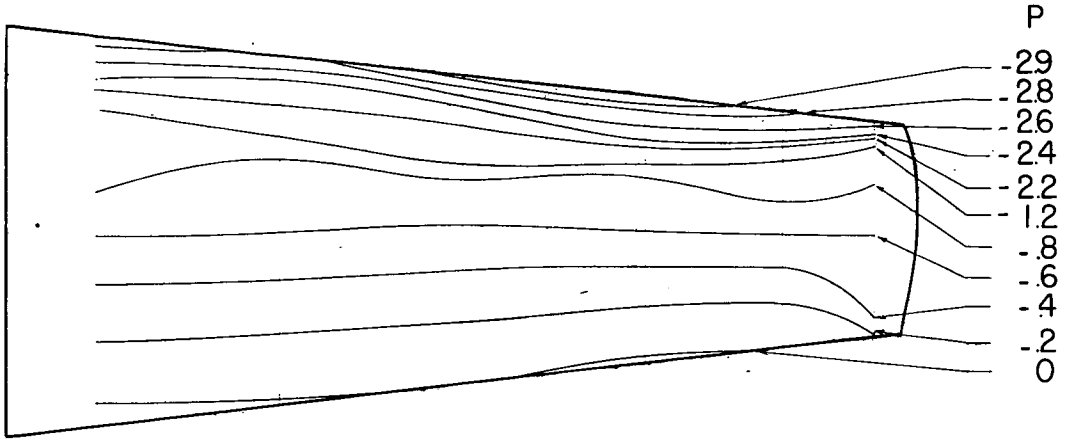

(d) $\alpha = 12.1^{\circ}$.

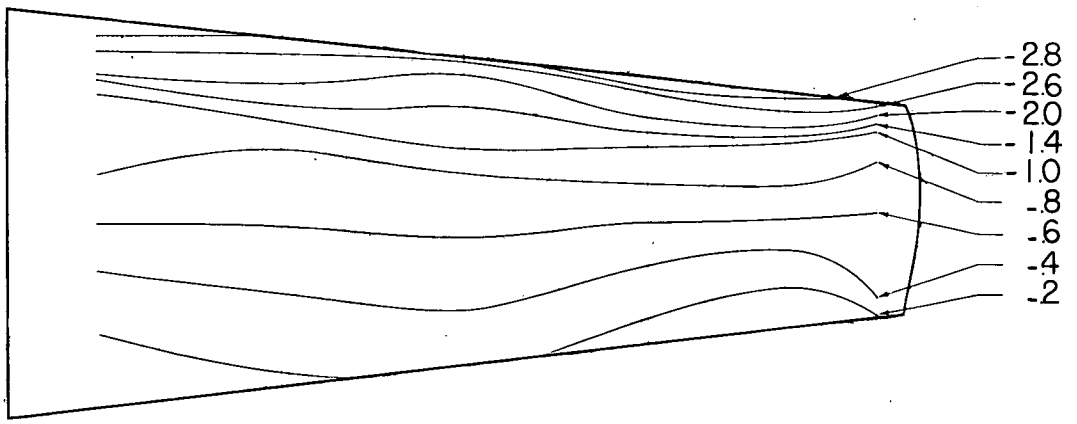

(e) $\alpha = 12.4^{\circ}$.

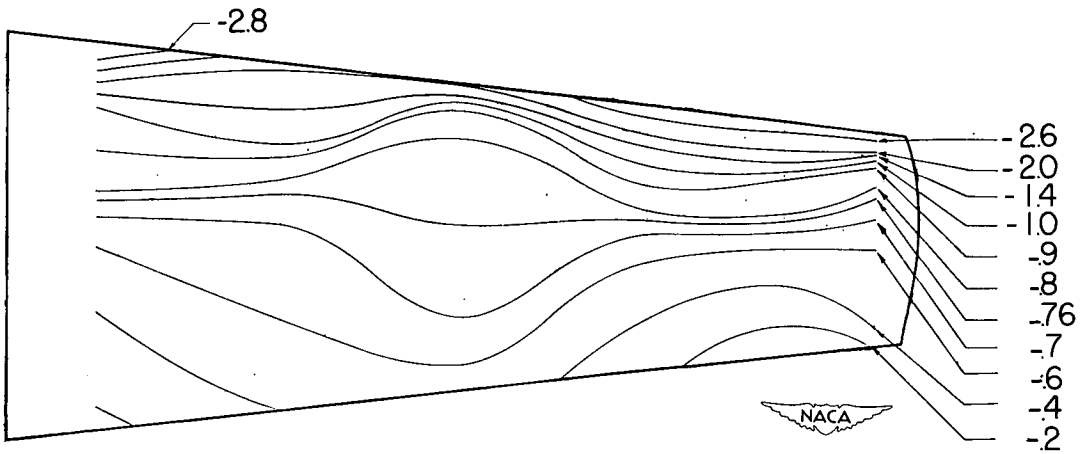

(f) $\alpha = 13.4^{\circ}$.

Figure 15.– Concluded.

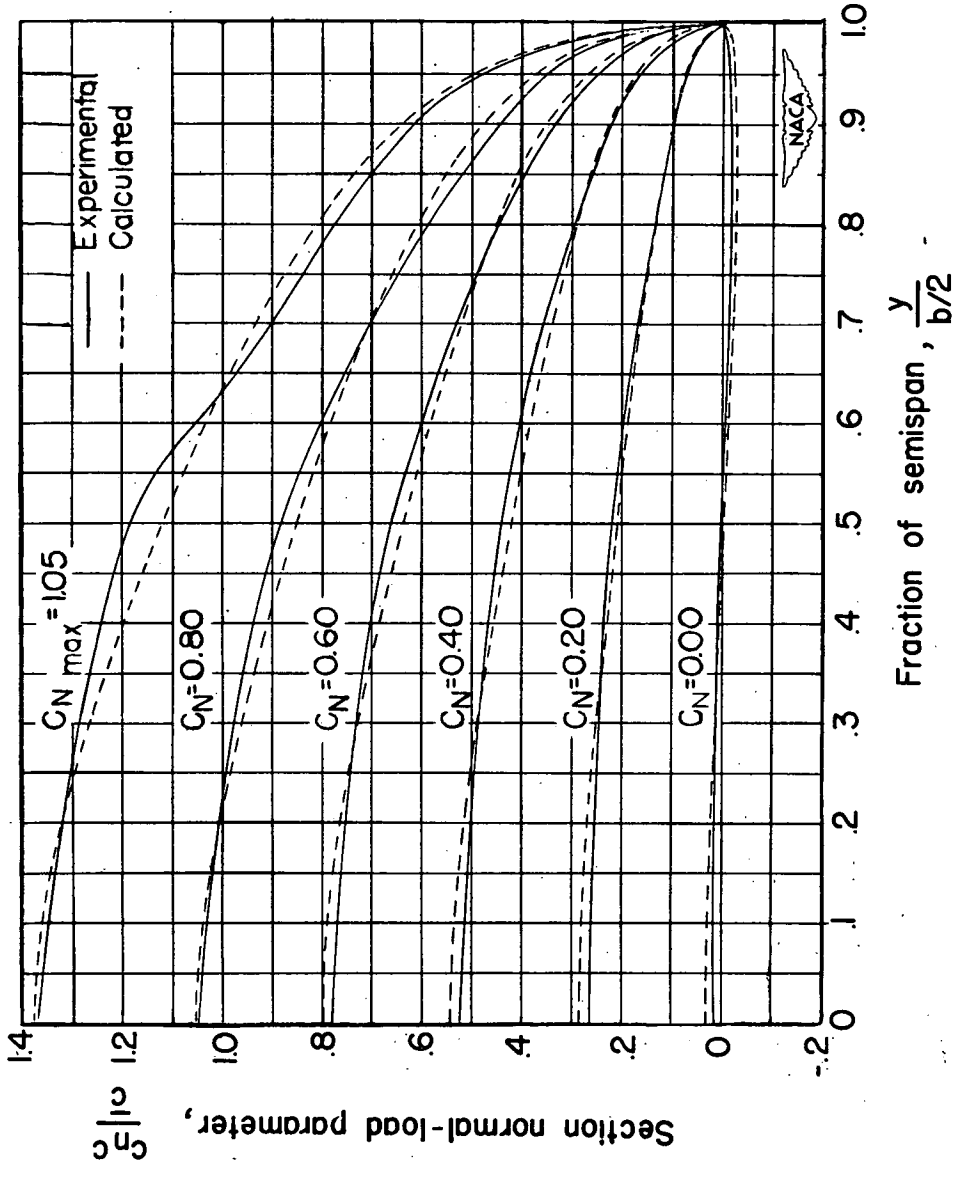

(a) M_0 = 0.20.

Figure 16.- Variation of experimental and calculated span-load distributions with normal-force coefficient for several Mach numbers.

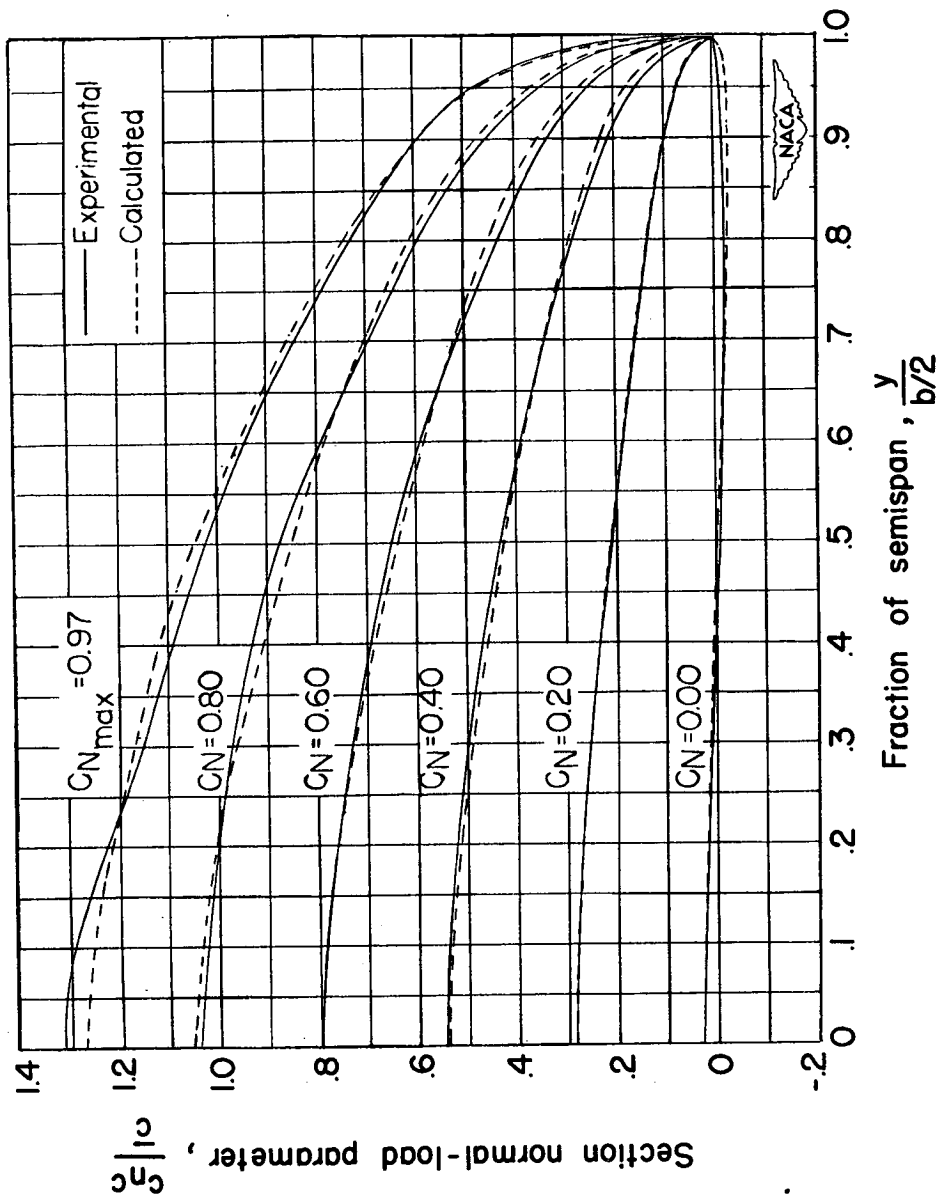

(b) M_o = 0.40.

Figure 16.- Continued.

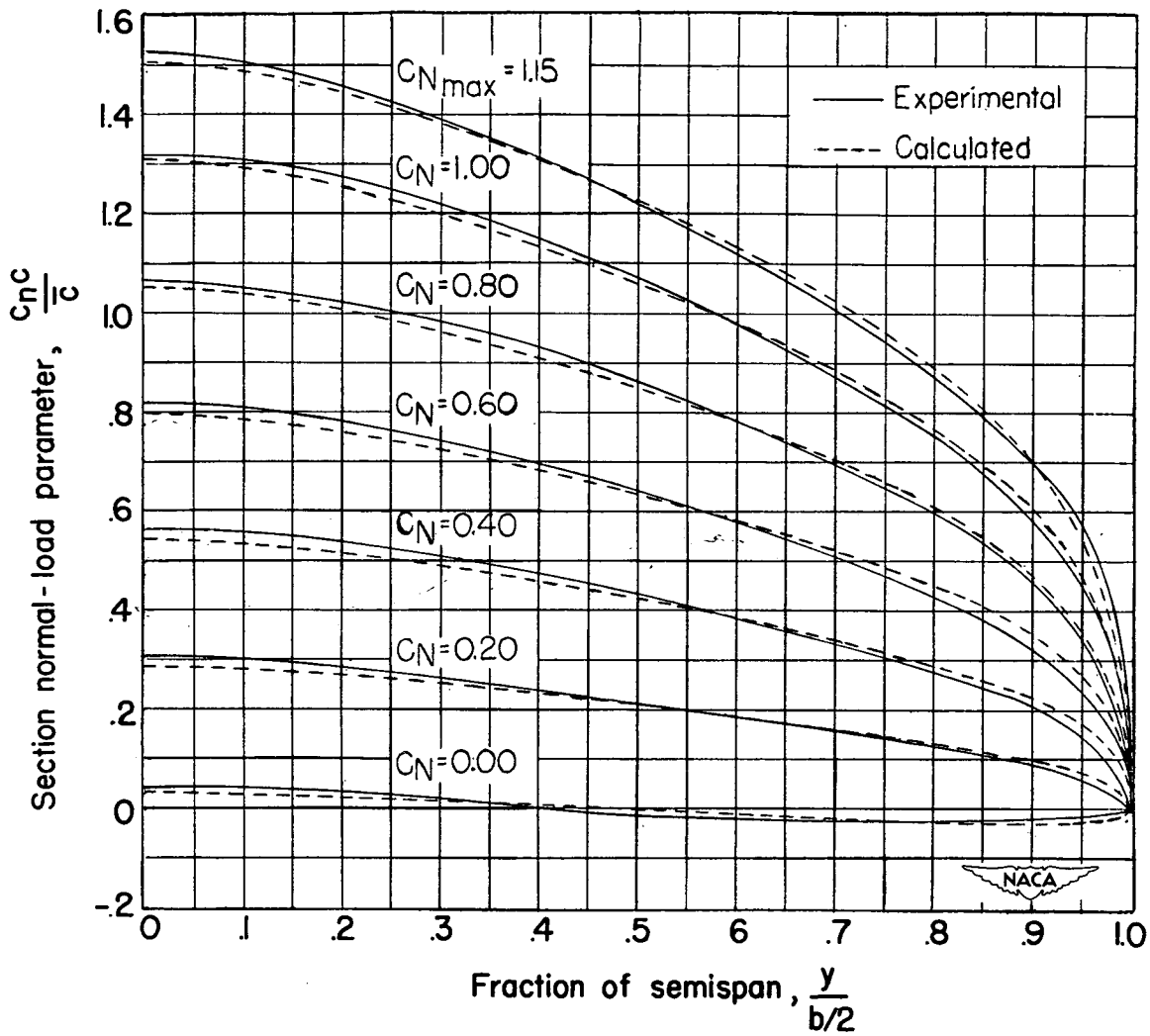

(c) $M_o = 0.60$.

Figure 16.– Concluded.

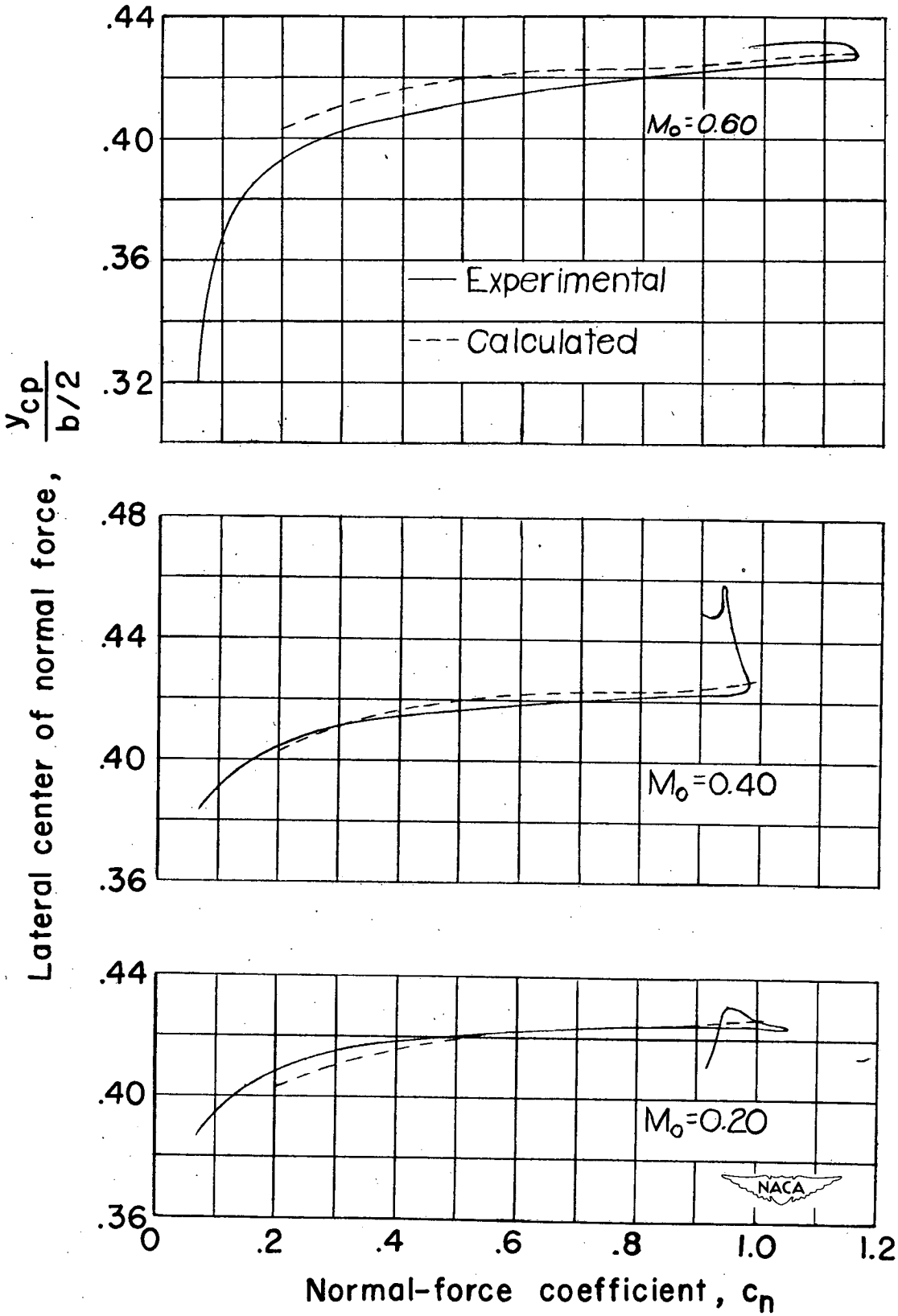

Figure 17.– Variation of experimental and calculated centers of normal force with normal-force coefficient for several Mach numbers.

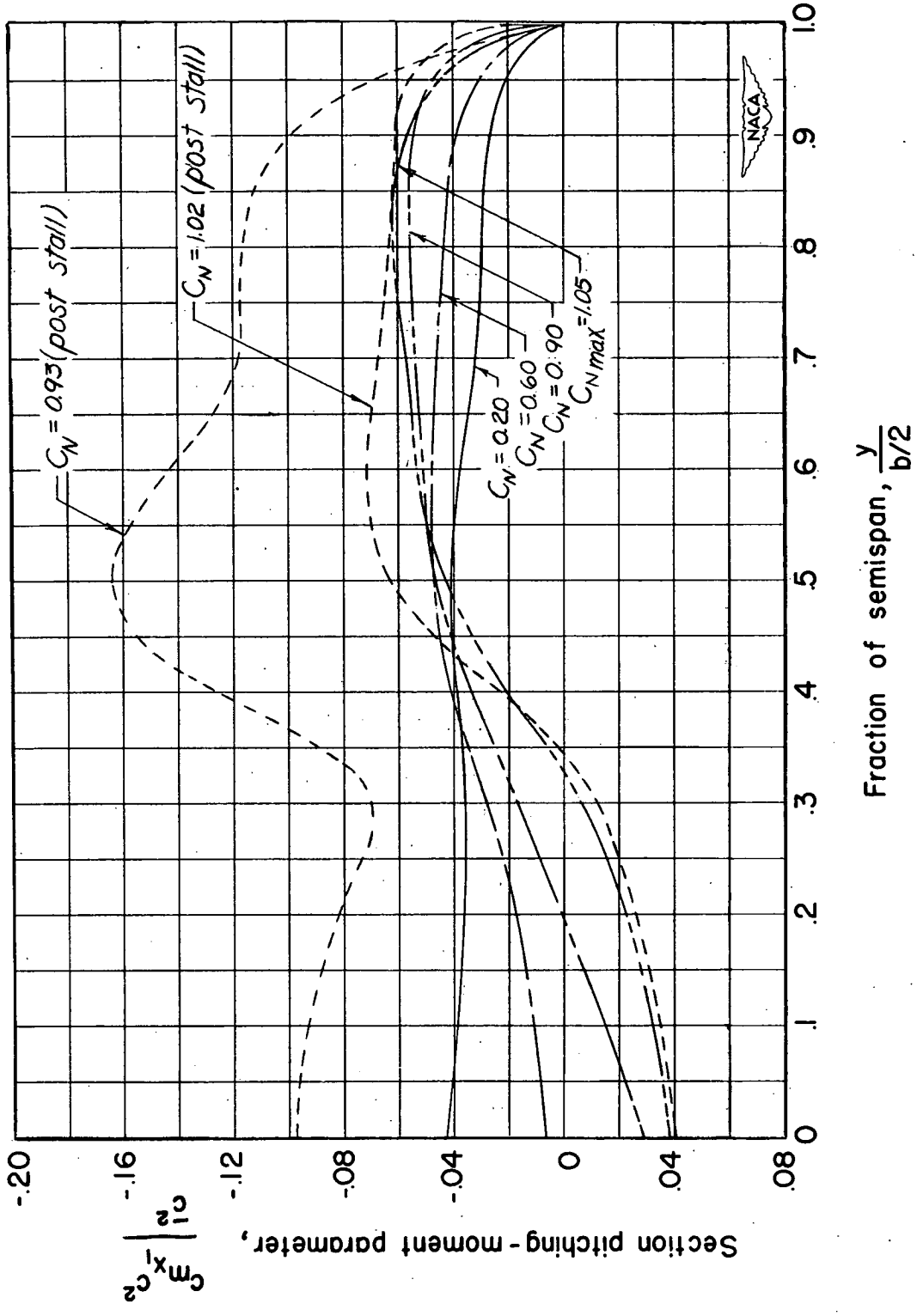

(a) $M_0 = 0.20$.

Figure 18.- Spanwise variation of section pitching-moment parameters with normal-force coefficient for several Mach numbers.

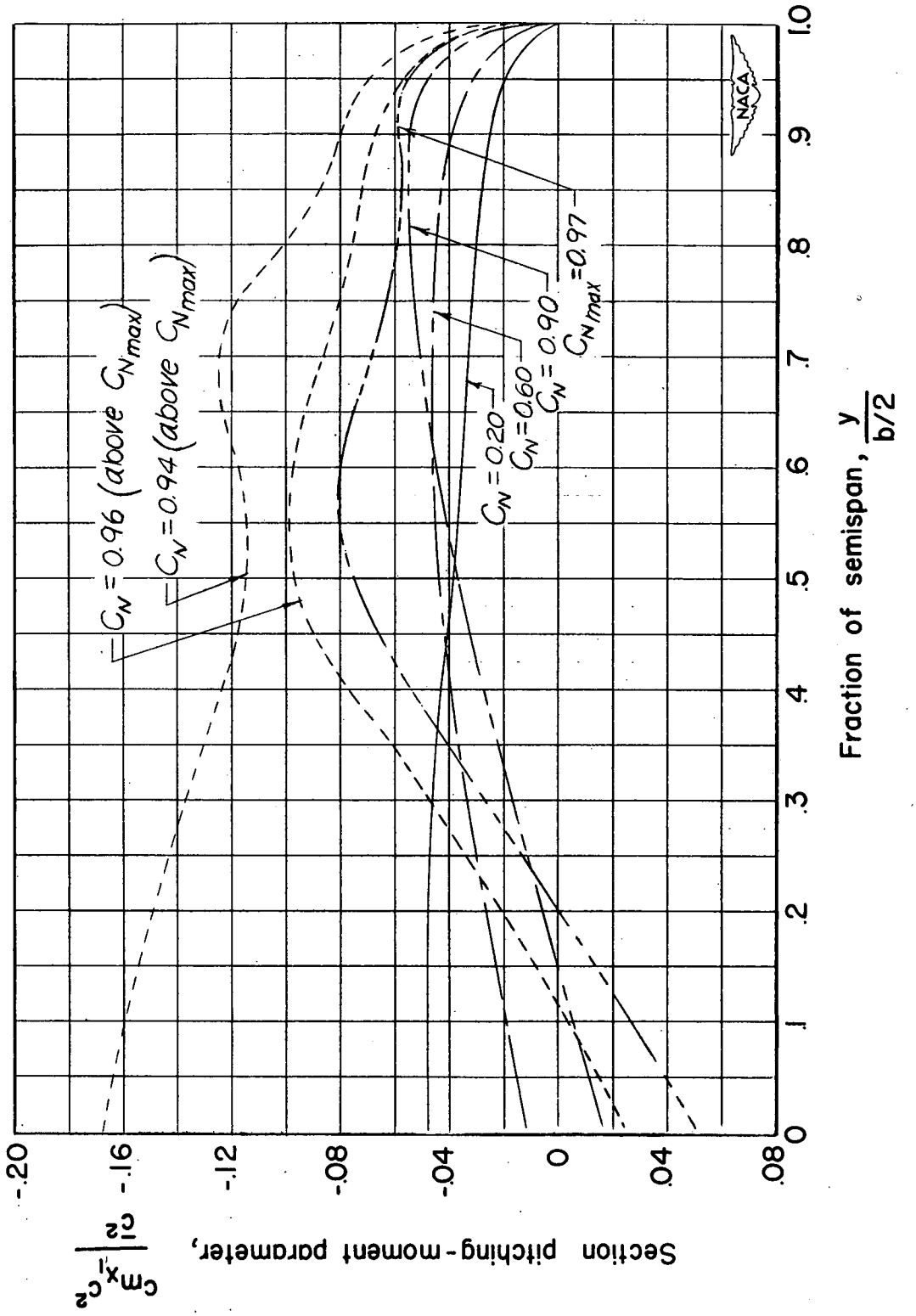

(b) $M_o = 0.40$.

Figure 18.- Continued.

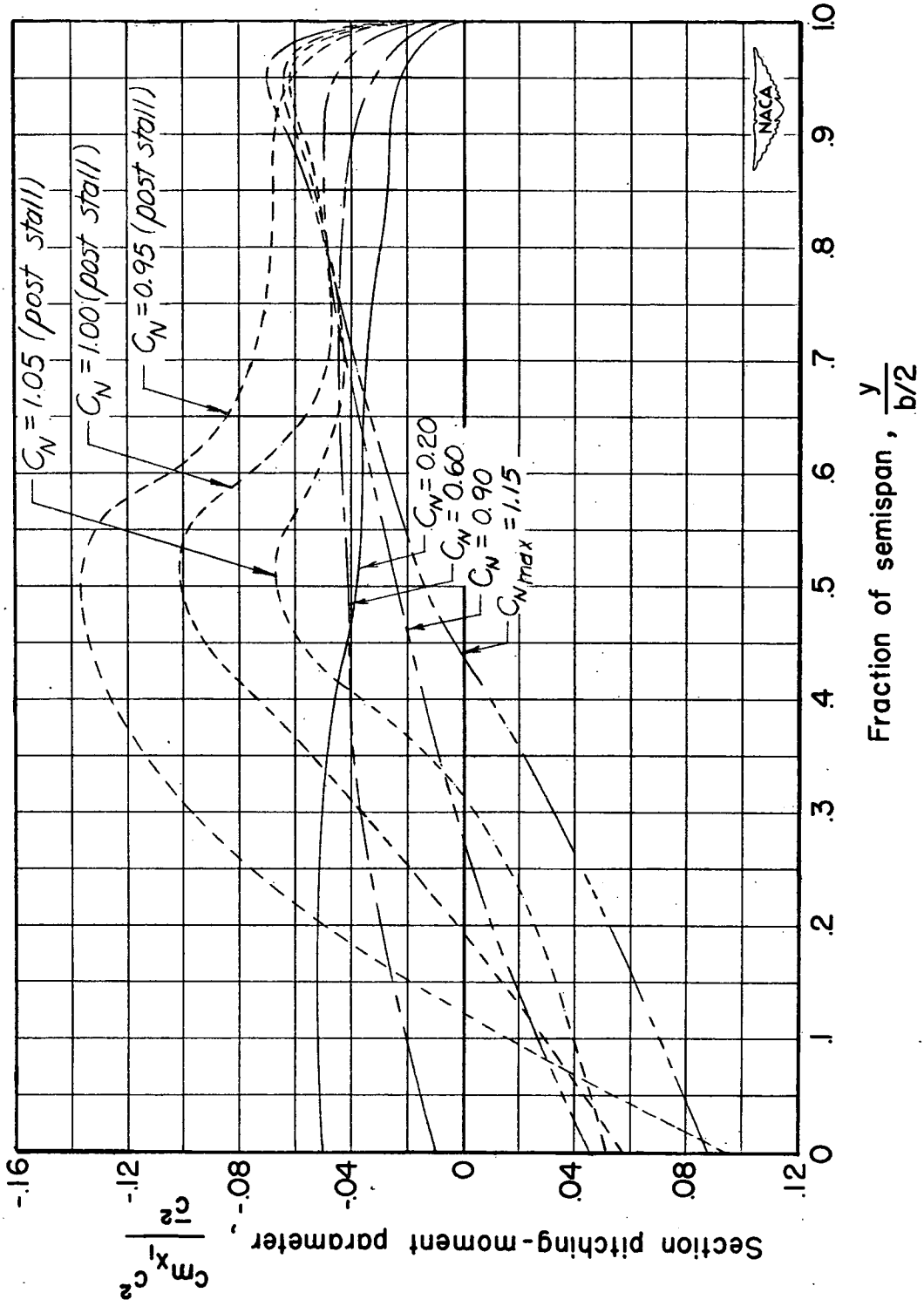

(c) $M_0 = 0.60$.

Figure 18.- Concluded.

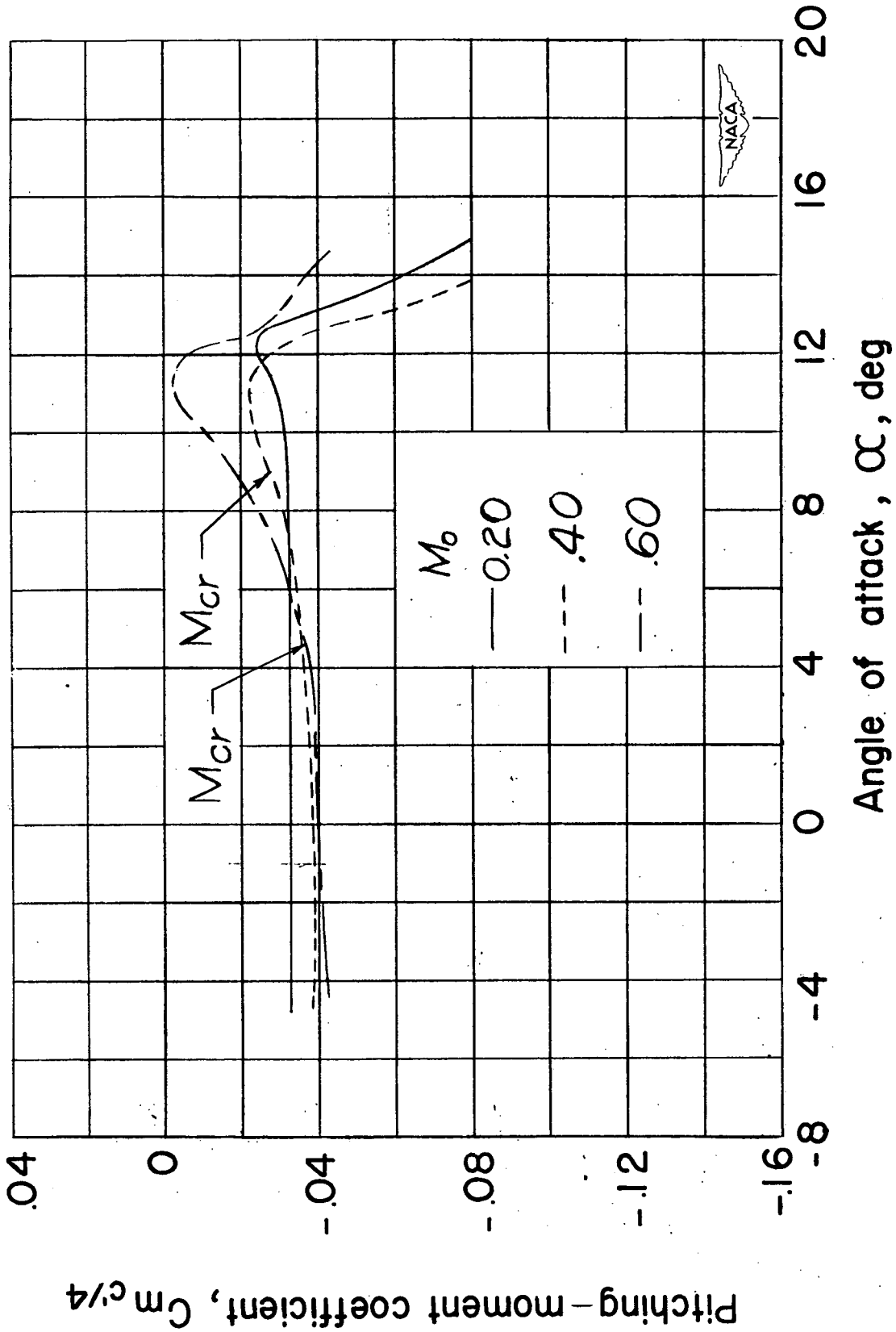

Figure 19.- Effect of Mach number on the variation of pitching-moment coefficient with angle of attack.

Abstract

The effects of compressibility on the lift, pressure, pitching-moment, and load characteristics of a 12-foot tapered wing having NACA 64-210 airfoil sections and an aspect ratio of 6 is presented for Mach numbers up to 0.60 and an angle-of-attack range of -4° up through the stall.

Abstract

The effects of compressibility on the lift, pressure, pitching-moment, and load characteristics of a 12-foot tapered wing having NACA 64-210 airfoil sections and an aspect ratio of 6 is presented for Mach numbers up to 0.60 and an angle-of-attack range of -4° up through the stall.

Abstract

The effects of compressibility on the lift, pressure, pitching-moment, and load characteristics of a 12-foot tapered wing having NACA 64-210 airfoil sections and an aspect ratio of 6 is presented for Mach numbers up to 0.60 and an angle-of-attack range of -4° up through the stall.

Abstract

The effects of compressibility on the lift, pressure, pitching-moment, and load characteristics of a 12-foot tapered wing having NACA 64-210 airfoil sections and an aspect ratio of 6 is presented for Mach numbers up to 0.60 and an angle-of-attack range of -4° up through the stall.

West, F. E., Jr., and Himka, T.

NACA

Effects of Compressibility on Lift and Load Characteristics of a Tapered Wing of NACA 64-210 Airfoil Sections up to a Mach Number of 0.60.

By F. E. West, Jr., and T. Himka

NACA TN No. 1877
May 1949

(Abstract on Reverse Side)

NACA

NACA

NACA